J BONE ONCOL 43 (2023) 100506

Contents lists available at ScienceDirect

Journal of Bone Oncology

journal homepage: www.elsevier.com/locate/jbo

Research Paper

The role of mitochondria-related lncRNAs in characterizing the immune landscape and supervising the prognosis of osteosarcoma

Yiming Zhang [a,1], Nan Ru [a,b,1], Zhaowen Xue [a,1], Wenyi Gan [a], Ruilin Pan [a], Zelin Wu [a], Zihang Chen [a,c], Huajun Wang [a,*], Xiaofei Zheng [a,*]

[a] Department of Sports Medicine, The First Affiliated Hospital, Guangdong Provincial Key Laboratory of Speed Capability, The Guangzhou Key Laboratory of Precision Orthopedics and Regenerative Medicine, Jinan University, Guangzhou, China
[b] Guangdong Engineering Research Center of Chinese Medicine & Disease Susceptibility, International Cooperative Laboratory of Traditional Chinese Medicine Modernization and Innovative Drug Development of the Chinese Ministry of Education, Guangdong Province Key Laboratory of Pharmacodynamic Constituents of Traditional Chinese Medicine and NewDrugs Research, Guangzhou, China
[c] Department of psychology, Li Ka Shing Faculty of Medicine, State Key Laboratory of Brain and Cognitive Sciences, The University of Hong Kong, Hong Kong, China

HIGHLIGHTS

- We investigated the co-expression network of mitochondria-related genes and lncRNAs.
- An accurate mitochondria-related lncRNA signature is proposed for osteosarcoma.
- This lncRNA signature facilitates prognostic evaluation in osteosarcoma.
- This lncRNA signature effectively predicts the immune landscape in osteosarcoma.
- We highlight the multifaceted role of core mitochondria-related lncRNAs in pan-cancer.

ARTICLE INFO

Keywords:
Osteosarcoma
lncRNA
Mitochondria
Immune infiltration
Personal treatment

ABSTRACT

Mitochondrial damage is related to the functional properties of immune cells as well as to tumorigenesis and progression. Nevertheless, there is an absence concerning the systematic evaluation of mitochondria-associated lncRNAs (MALs) in the immune profile and tumor microenvironment of osteosarcoma patients. Based on transcriptomic and clinicopathological data from the TARGET database, MAL-related patterns were ascertained by consistent clustering, and gene set variation analysis of the different patterns was completed. Next, a MAL-derived scoring system was created using Cox and LASSO regression analyses and validated by Kaplan-Meier and ROC curves. The GSEA, ESTIMATE, and CIBERSORT algorithms were utilized to characterize the immune status and underlying biological functions in the different MAL score groups. MAL-derived risk scores were well stabilized and outperformed traditional clinicopathological features to reliably predict 5-year survival in osteosarcoma cohorts. Moreover, patients with increased MAL scores were observed to suffer from poorer prognosis, higher tumor purity, and an immunosuppressive microenvironment. Based on estimated half-maximal inhibitory concentrations, the low-MAL score group benefited more from gemcitabine and docetaxel, and less from thapsigargin and sunitinib compared to the high-MAL score group. Pan-cancer analysis demonstrated that six hub MALs were strongly correlated with clinical outcomes, immune subtypes, and tumor stemness indices in various common cancers. Finally, we verified the expression patterns of hub MALs in osteosarcoma with qRT-PCR. In summary, we identified the crosstalk between prognostic MALs and tumor-infiltrating immune cells in osteosarcoma, providing a potential strategy to ameliorate clinical stratification management.

* Corresponding authors at: Department of Sports Medicine, The First Affiliated Hospital, Guangdong Provincial Key Laboratory of Speed Capability, The Guangzhou Key Laboratory of Precision Orthopedics and Regenerative Medicine, Jinan University, Guangzhou 510000, China.
E-mail addresses: hjwang@jnu.edu.cn (H. Wang), xfzheng@jnu.edu.cn (X. Zheng).
[1] These authors have contributed equally to this work.

https://doi.org/10.1016/j.jbo.2023.100506
Received 30 May 2023; Received in revised form 24 September 2023; Accepted 3 October 2023
Available online 5 October 2023

1. Introduction

Osteosarcoma is the most common primary malignant bone tumor in adolescents and children, with a worldwide prevalence of four to five per million [1,2]. The initial symptoms of osteosarcoma commonly consist of pain, swelling, and the potential for local tenderness and inflammation [3–5]. In later stages, symptoms may include restricted mobility of the joint and the occurrence of pathologic fractures [6]. Unfortunately, in the early stages of osteosarcoma, symptoms are often mistaken for growing pains or intense exercise-induced discomfort in the adolescent population, thereby delaying diagnosis [7–9]. In addition, Osteosarcoma is a highly malignant and invasive disease, making it difficult for patients to capture the best opportunities for treatment [10]. It spreads easily through the bloodstream in its initial phases, and the resulting pulmonary metastases are a major cause of death for patients [11]. Although long-term survival rates for patients with situ lesions have been maintained above 60 % since the 1970 s through various treatment modalities such as surgical resection and chemotherapy, there has been no improvement in long-term survival rates for patients who have developed lung metastases [12,13]. Therefore, there is an urgent demand to develop accurate and reliable molecular biomarkers for early diagnosis and prognosis.

The tumor microenvironment (TME) is a complex, highly heterogeneous, and dynamic integrated system, mainly composed of tumor cells, cancer-associated fibroblasts, tumor-infiltrating immune cells (TICs), and microvasculature [14,15]. During tumorigenesis and progression, strongly metabolically active cancer cells interfere with immune cell function in the TME by consuming nutrients and producing immunosuppressive metabolites [16]. Mitochondria are the targets and feedback centers of various energy metabolism regulators, where metabolic processes such as oxidative phosphorylation (OXPHOS), tricarboxylic acid cycle, and lipid metabolism are located [17,18]. Reactive oxygen species (ROS) are unstable molecules produced by the NADPH oxidase and cytochrome P450 system in mitochondria during OXPHOS with oxygen, providing another source of genomic instability [19,20]. Mitochondria are both the origin and target of ROS, and increased levels of ROS lead to mitochondrial dysfunction, which in turn further inflates ROS levels [21–23]. Moreover, as the site of energy production using oxygen, mitochondria are central to intracellular oxidative stress injury and the convergence point of numerous programmed cell death pathways [24]. Such as ferroptosis, a novel form of regulatory necrotic process triggered by the imbalance of iron-dependent lipid peroxidation, is closely related to the disruption of mitochondrial redox homeostasis [25,26]. Noteworthy, during tumor metabolic reprogramming, structural and functional alterations of mitochondria themselves affect tumor cell status and play a broad regulatory role in tumor proliferation, immune escape, invasion, migration, angiogenesis, and drug resistance [27]. As reported by Toki et al. viability and multiplication of osteosarcoma cells are dependent on the regulation of PARP-1/AIF pathway-dependent apoptosis by the mitochondrial BIG3-PHB2 complex [28]. Another study showed that a novel arsenic-based mitochondrial toxin, PENAO, could induce oxidative stress and mitochondrial membrane potential depolarization, which synergistically enhanced ROS production and mitochondrial-mediated apoptosis with the pyruvate dehydrogenase kinase inhibitor dichloroacetate, subsequently causing tumor cell proliferation and cycle arrest [29]. Notably, impaired OXPHOS processes, abnormal mitochondrial metabolism, and autophagy drive the homeostatic abnormalities and depletion programs of immune cells in the TME [30]. Mitochondria play a crucial role in altering the metabolic pattern of T cells to achieve the desired immune response. Mitochondrial disorder-causing defective T-cell activation could lead to immune surveillance impairment and expedite tumor progress [31]. Tumor-infiltrating T lymphocytes frequently exhibit mitochondrial damage accompanied by a loss of redox balance, which limits their proliferation and self-renewal [32]. A major challenge for immune checkpoint blockade (ICB) and adoptive cell transfer (ACT) is the eventual development of T cell failure and senescence, and these restrictions can be overcome by metabolic stabilization improving T cell adaptability and lifespan in TME [33]. Therefore there is a need for an in-depth exploration of the crosstalk between mitochondria and immune cells to provide more possibilities for early diagnosis and treatment of osteosarcoma.

Long non-coding RNAs (lncRNAs) are widely known as crucial gene regulators of cell biology, whose crosstalk with mitochondria is of mounting attention. As reported, lncRNA Tug1 affected mitochondrial Ca2 + transport and myogenesis-related transcriptional networks regulating skeletal muscle responses to motor stimuli [34]. Another study noted that lncDACH1 is highly expressed in high glucose-treated cardiomyocytes, which exacerbates diabetic cardiomyopathy by increasing ubiquitination-mediated sirtuin3 degradation to promote mitochondria-derived ROS levels and apoptosis [35]. LncRNA Punisher modulated H2O2-induced vascular smooth muscle cell apoptosis and mitochondrial dynamics via the miR-664a-5p/OPA1 axis, thereby attenuating the development of atherosclerosis [36]. Research by Wo et al. demonstrated that the lncRNA HABON interacted with the VDAC1 to dampen mPTP opening and significantly enhanced mitochondrial activity, resulting in the inhibition of tumor cell apoptosis [37]. Furthermore, lncRNAs intimately interact with other molecules to regulate osteosarcoma invasion, metastasis, EMT, and prognosis [38]. The study of Li et al. demonstrated that lncSNHG14 overexpression competitively binds miR-206 to protect SLC7A11 from degradation, thereby inhibiting ferroptosis in osteosarcoma cells and then promoting chemoresistance of nutlin3a [39]. LINC00629 promotes osteosarcoma development and metastatic spread by regulating KLF4 stability and endoplasmic reticulum stress-induced apoptosis [40]. Notably, ever-increasing studies have addressed lncRNAs as biomarkers to predict therapeutic response in osteosarcoma, including m6A-associated, Ferroptosis-associated, and immune-associated lncRNA models [41–43]. However, it is poorly understood the implications of mitochondria-associated lncRNAs on clinical stratification management, immune response, tumor microenvironment, and fate regulation of osteosarcoma cells.

Considering the essential value of lncRNAs and mitochondria in osteosarcoma, bioinformatics analysis was deployed to mine potentially dysregulated lncRNAs involving mitochondria. We established a novel MAL prognostic index for predicting outcomes in osteosarcoma patients and probed more accurate molecular phenotypes and corresponding TME profiles in osteosarcoma. This study may provide a basis for investigating the crosstalk between mitochondria and its relevant lncRNAs in the molecular regulatory mechanisms of osteosarcoma.

2. Materials and methods

2.1. Sample data download and collation

The osteosarcoma transcriptome data and clinical data were downloaded from the TARGET database (https://ocg.cancer.gov/programs/target) and included mRNAs and lncRNAs. The clinical data were sorted to include futime (survival time), fustat (survival status), sex, age at diagnosis in days, metastatic and non-metastatic. After excluding patients with unavailable gene expression matrices, we included data from 88 cases to ensure the reliability of the study results. A dataset of 396 normal musculoskeletal samples was obtained from the GTEx database (https://www.gtexportal.org/home/) as the control [44,45]. We consolidated the above gene expression matrices into one expression matrix (457 samples in total) and bias-corrected the merged data using the “sva” package [44,46]. Transcriptome expression and clinical datasets of 33 tumor types were downloaded from the Cancer Genome Atlas (TCGA) cohort (https://portal.gdc.cancer.gov/).

2.2. Acquisition of hub MALs associated with prognosis in osteosarcoma

The mitochondria-related genes (MRGs) as shown in Supplementary Table S1 were fetched from the MitoCarta3.0 database (https://www.broadinstitute.org/mitocarta), which provides 1136 genes encoding the mitochondrial proteome, including mitochondrial sub-organelle localization and pathway annotations [47]. Regarding the above gene list, we extracted the differential expression values of MRGs with the "limma" package. Following the "clusterProfiler" package, gene ontology (GO) and Kyoto Encyclopedia of Genes and Genomes (KEGG) pathway analyses were performed to investigate the cellular and molecular functions of MRGs. In order to assess the correlation between the mitochondria-related genes and lncRNAs, we performed Pearson correlation analysis using the "corrplot" package and defined lncRNAs with P value < 0.001 and absolute correlation coefficient > 0.4 as MALs [48,49]. The network of MRGs and their co-expression MALs was generated via the "igraph" package. Univariate Cox regression was undertaken for further screening of prognostic MRGs or MALs using the "survival" package. Hazard ratio (HR) greater than 1 suggested an inferior prognosis and vice versa.

2.3. Consensus clustering analysis and risk stratification system construction based on MALs

With MALs screened by Cox regression, we implemented an unsupervised clustering approach to identify the heterogeneity of MAL molecular patterns in osteosarcoma using the "ConsensusClusterPlus" package. Gene set variation analysis (GSVA) and single-sample gene set enrichment analysis (ssGSEA) were applied to quantify the pathway enrichment scores and levels of TICs for different MAL subtypes by the "GSVA", "GSEABase", "ggpubr", and "reshape2″ packages. The least absolute shrinkage and selection operator regression (LASSO) was deployed to further screen pivotal MALs and refine the risk stratification system. MAL scores = Σ (coefi × Expi) (coef: coefficient, Exp: MAL expression level). Using the "caret" R package, the TARGET samples were randomly divided into training and test groups in a 1:1 ratio. The median MAL score was specified as the cut-off value for case classification in each cohort. Kaplan-Meier (KM) survival analyses were carried out to estimate the overall survival (OS) of both cohorts with the "timeROC" package. The reliability of the MAL scores was authenticated by receiver operating characteristic (ROC) curves and these analyses were repeated in the train, test, and entire cohorts.

2.4. Independent prognostic analysis, stratified analysis, and clinical correlation analysis

To exclude the influence of other clinical characteristics, we used COX regression to determine whether the MAL score was an independent prognostic factor. We extracted clinical information from the TARGET dataset for osteosarcoma patients and subdivided it for each parameter. Specifically, two groups were classified according to age ($\leq$18 and $>$ 18 years), gender (female and male), and metastatic status (metastatic and non-metastatic). The nomogram was configured using the "rms" package in combination with clinical features and MAL score to assess the survival probability of osteosarcoma patients. The accuracy of the nomograms was also estimated with the corresponding calibration curves. KM analysis stratified by clinicopathological characteristics was subsequently performed. The chi-square was applied to appraise the relationship between the MAL score and clinical parameters.

2.5. Comparative analysis of prognostic features and clinical variables

The lncRNA prognostic models included in the comparative analysis were obtained from published studies, which we named according to the authors' names as Yang [50], Gong [51], Wang [52], and Bu [53] scoring systems. We calculated the concordance index (C-index) and area under the ROC curve (AUC) values of different prognostic signatures and clinical variables by the "Pec", "timeROC", and "dplyr" packages for superiority comparison.

2.6. Application of MAL scoring system in predicting TME and response to chemotherapy/immunotherapy

After computing TME scores and tumor purity between the high- and low-MAL score groups with the "estimation" package, the Wilcoxon rank sum test was availed to resolve the discrepancy between both groups. TICs and stromal cells are receiving increasing concern as major cellular components of TME influencing neoplastic progression [54]. Therefore, the CIBERSORT deconvolution algorithm was adopted to accurately quantify the proportions of TICs (22 different cell types) depending on the gene expression profiles of each osteosarcoma. The Spearman test was then carried out to investigate the correlation between the MAL score and immune cell content. Single sample gene set enrichment analysis (ssGSEA) was applied to explore the activation degree of TICs and immune-related pathways between two MAL score groups. To assess discrepancies in immunotherapy response, we compared the expression of human leukocyte antigen (HLA) genes and immune checkpoint genes (ICGs) in patients with high or low MAL scores. Since immunotherapy may achieve better efficacy in combination with targeted therapy or chemotherapy, we assessed the half-maximal inhibitory concentration (IC50) of several targeted agents or chemotherapeutic agents that may benefit osteosarcoma patients using information from the Cancer Genome Project (CGP) database (https://www.sanger.ac.uk/genetics/CGP/) to predict the sensitivity of these drugs in diverse MAL score groups. In principle, lower IC50 values and higher ICG expression predicted better sensitivity to chemotherapy and immunotherapy, respectively [55–57]. The biological characteristics of the two MAL scoring groups were further elucidated using the GSEA algorithm with reference to genome collections (c2.cp.kegg.v7.4.symbols.gmt and c5.go.v7.4.symbols.gmt) obtained from the MSigDB database (https://www.gsea-msigdb.org/gsea/index.jsp).

2.7. Three-dimensional structure prediction and subcellular localization analysis

AlphaFold, an artificial intelligence tool that applies deep learning to structural and genetic data, can accurately predict protein structures based on amino acid sequences while evaluating the confidence of its predictions [58]. We estimate the three-dimensional (3D) structure of core MRGs by AlphaFold to promote our understanding of the basic cellular composition. The Human Protein Atlas (HPA, https://www.proteinatlas.org/) and lncATLAS databases (https://lncatlas.crg.eu/) were instrumental in determining the subcellular localization of core MRGs and MALs, respectively.

2.8. Pan-cancer analysis

The Cancer Genome Atlas (TCGA) (https://portal.gdc.cancer.gov/) Database is a cancer research project established by the National Cancer Institute (NCI, National Cancer Institute) and National Human Genome Research Institute (NHGRI, National Human Genome Institute), which provides a large-scale reference database for cancer research by collecting and organizing various cancer-related multi-omics data, including genomes, transcriptomes, epigenomes, and proteomes [59]. Transcriptome expression and clinical datasets of 33 tumor types were downloaded from the TCGA cohort. The abbreviations of 33 tumor types are shown in Supplementary Table S2. The MAL expression information between 33 tumor types and matched normal tissues was extracted and analyzed for significant differences with the Wilcoxon test by the "ggpubr" package. The association between MAL expression and OS of patients with 33 cancer types was subsequently examined with KM analysis and univariate cox regression. Correlations between critical

MALs and cancer immune subtypes were determined with Kruskal-Wallis tests. To investigate the relationship between MAL and tumor stemness in different cancer types, correlation analysis between key MAL and RNA stemness scores (RNAss) or DNA methylation stemness scores (DNAss) was applied by the Spearman correlation test.

2.9. Cell culture and quantitative real-time polymerase chain reaction (qRT-PCR)

Three osteosarcoma cell lines and one osteoblast cell line were used in this study: MG63, U2OS, MNNG/HOS, and hFOB1.19. All cell lines were obtained through the Cell Bank of the Chinese Academy of Sciences (Shanghai, China) and cultured according to the instructions. Total RNA was prepared using RNA-easyTM isolation reagent (Vazyme Biotech Co.,

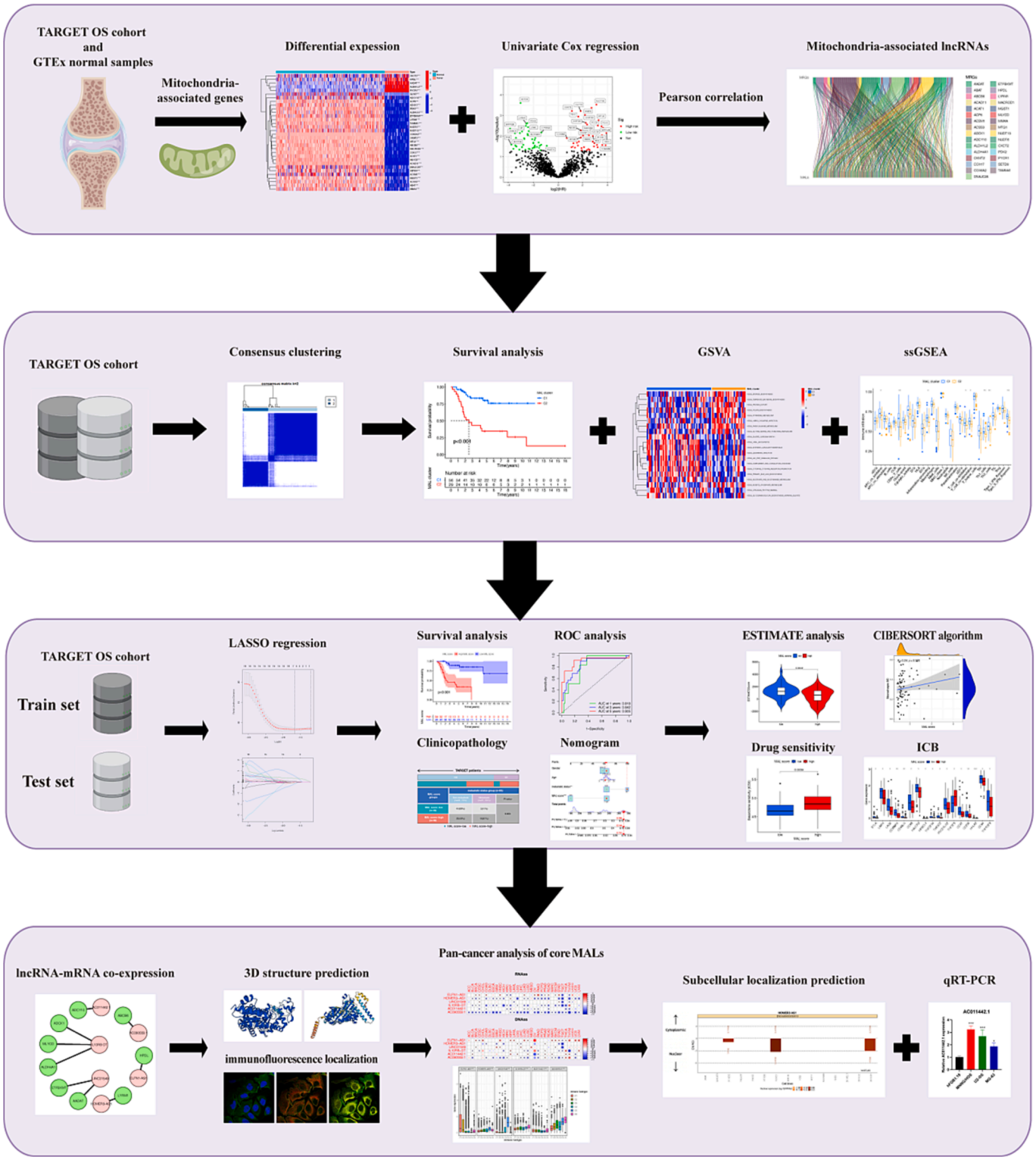

Fig. 1. Flow chart of this study.

Ltd., Nanjing, China) and then reverse transcribed into cDNA with HiScript III RT SuperMix (Vazyme, China). Finally, qRT-PCR was performed using the UltraSYBR Mixture Kit (CWBIO, China). GAPDH was set as internal control and relative gene expression was calculated by the 2–ΔΔCt method. Primer sequences for relevant genes are described in Supplementary Table S3.

2.10. Statistical analysis

This study was based on R software (version 4.2.1) and GraphPad Prism 8.0 to analyze the data and generate graphs. All experiments were performed at least three times independently. Continuous variables were expressed using the mean ± standard deviation. Statistical differences between groups were calculated by *t*-test or one-way ANOVA. $P < 0.05$ was considered statistically significant.

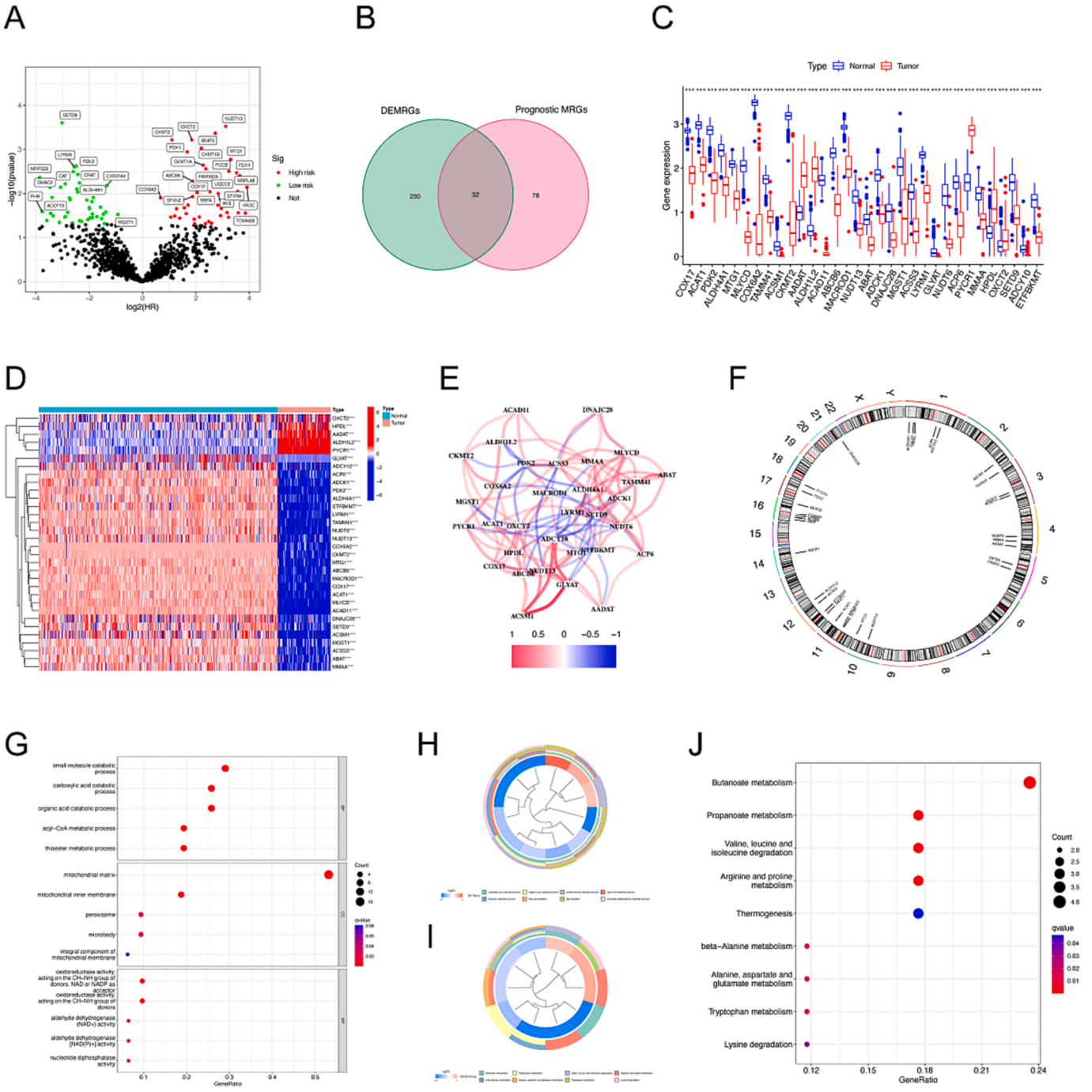

Fig. 2. Screening pivotal MRGs and corresponding functional enrichment analysis (A) Prognostic MRGs in osteosarcoma filtered by univariate Cox regression. (B) Determination of pivotal MRGs by intersecting differentially expressed MRGs with prognostic MRGs. (C-D) Boxplot (C) and heatmap (D) indicating differential expression levels of pivotal MRGs in osteosarcoma and normal tissues. (E) Interaction network of the 32 pivotal MRGs. (F) Locations of pivotal MRGs on the chromosome. (G-H) Gene Ontology enrichment analysis of pivotal MRGs. (I-J) Kyoto Encyclopedia of Genes and Genomes analysis of pivotal MRGs. MRGs, mitochondria-related genes; *p < 0.05; **p < 0.01; ***p < 0.001.

3. Results

3.1. Identification of hub MRGs and functional enrichment analysis

The flowchart of the integrated strategy was showed in Fig. 1. Under the cutoff criteria of |logFC| > 1 and FDR < 0.05, we collected 262 differentially expressed MRGs (DEMRGs) between osteosarcoma and normal tissues, of which 46 were upregulated and 216 were downregulated (Supplementary Table S4). The prognostic value of MRGs was determined by Cox regression analysis, revealing 52 MRGs with HR greater than 1 as negative prognostic factors and 58 MRGs with HR less than 1 as favorable prognostic factors (Supplementary Table S5, Fig. 2A). Subsequently, 32 core MRGs were harvested by intersecting DEMRGs and prognostic MRGs (Fig. 2B), whose expressions are depicted in Fig. 2C, D. We focused on the linkage of these hub MRGs. According to the co-expression network, ADCY10, GLYAT, and ACSM1 were the highest correlative regulators, suggesting their potential co-interaction (Fig. 2E). Fig. 2F illustrates the location of these MRGs on chromosomes, with the majority localized on chromosomes 1, 12, and 16. GO enrichment analysis demonstrated that most of these MRGs are enriched in the mitochondrial matrix, mitochondrial inner membrane, and small molecule catabolic process and affect OXPHOS-related molecular functions such as oxidoreductase activity, aldehyde dehydrogenase [NAD(P) +] activity, nucleotide diphosphatase activity (Fig. 2G, H). KEGG enrichment determined numerous underlying mechanisms related to amino acid metabolism, with “Butanoate metabolism”, “Propanoate metabolism” and “Valine, leucine, and isoleucine degradation” forming the first five significantly enriched pathways (Fig. 2I, J).

3.2. Screening of mitochondria-related lncRNAs in osteosarcoma

A total of 512 MALs were defined using Pearson correlations at strict screening criteria (correlation coefficient > 0.4 and P value < 0.001) (Fig. 3A, Supplementary Table S6), followed by the construction of a MAL-MRG co-expression network in osteosarcoma patients (Fig. 3B). After univariate Cox analysis, 58 MALs exerted a remarkable impact on patient outcomes, among which 11 were low-risk MALs, such as HOMER3-AS1, AC005332.4, and AC090559.1 (Fig. 3C). On the other hand, the remaining 23 were considered adverse indices, including SATB2-AS1, USP2-AS1, TBX2-AS1, and others (Fig. 3C). In exploring the MAL-PDL1 correspondence, varying degrees of positive or negative associations between HOMER3-AS1, LINC02298, LINC01549, AC010609.1, VPS9D1-AS1, AL161729.1, AC005332.4, AC090559.1 and PDL1 were detected (Fig. 3D).

3.3. Determination of MAL-related clusters and the characteristics of TICs

Based on the expression of prognostic-related MALs, we attempted to ascertain molecular subtypes of the TARGET cohort by applying consensus clustering analysis. The CDF graph reflected the ideal value of 2 for cluster number, whereby all osteosarcoma samples are separated into two MAL patterns, designated MAL cluster C1 – C2 (Fig. 4A). We discovered that these two clusters differ significantly in terms of MAL expression as presented in Fig. 4B. The clustering of MALs in PCA

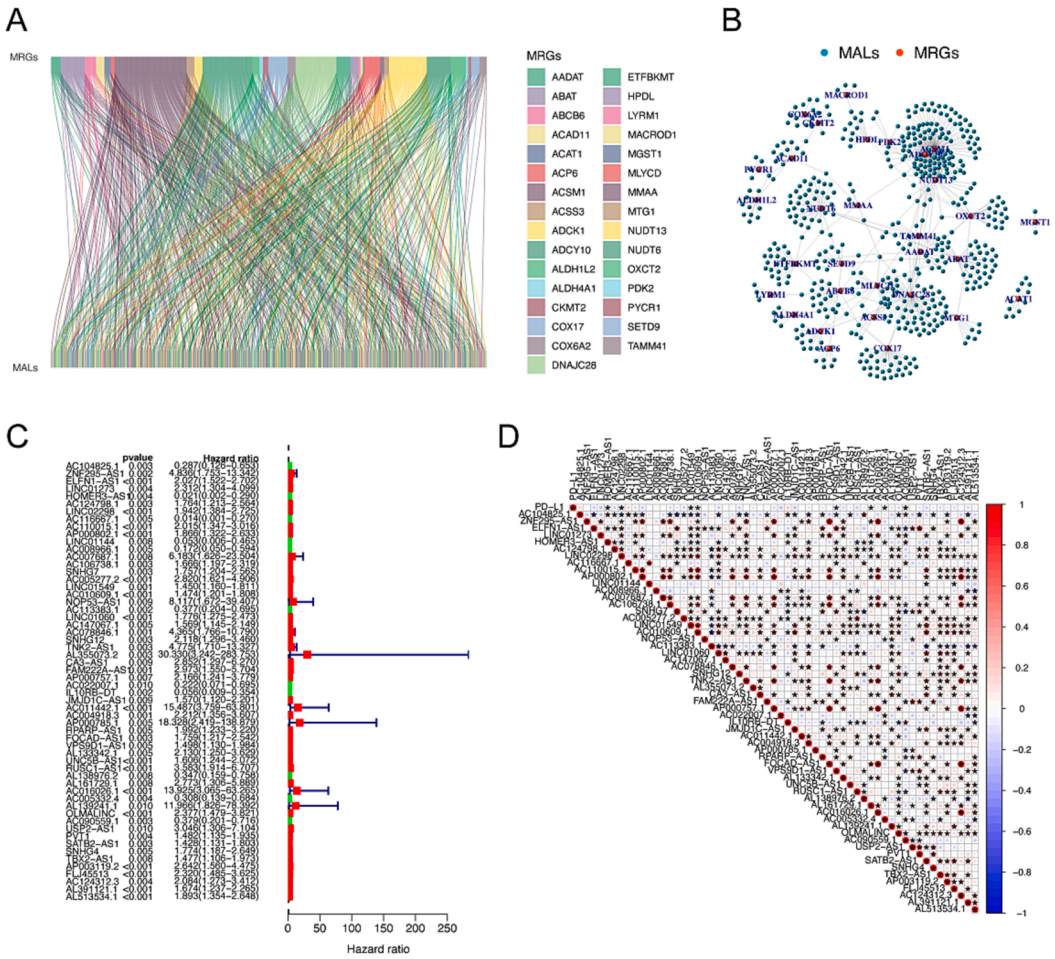

Fig. 3. Identification of prognostic MALs in osteosarcoma (A) Sankey diagram of the relationship between MALs and hub MRGs. (B) Co-expression network of correlated MALs and MRGs. (C) Forest plot of Cox regression analysis for prognostic MALs. (D) Correlation between MALs and PDL1 expression. MALs, mitochondria-related lncRNAs; MRGs, mitochondria-related genes. *p < 0.05.

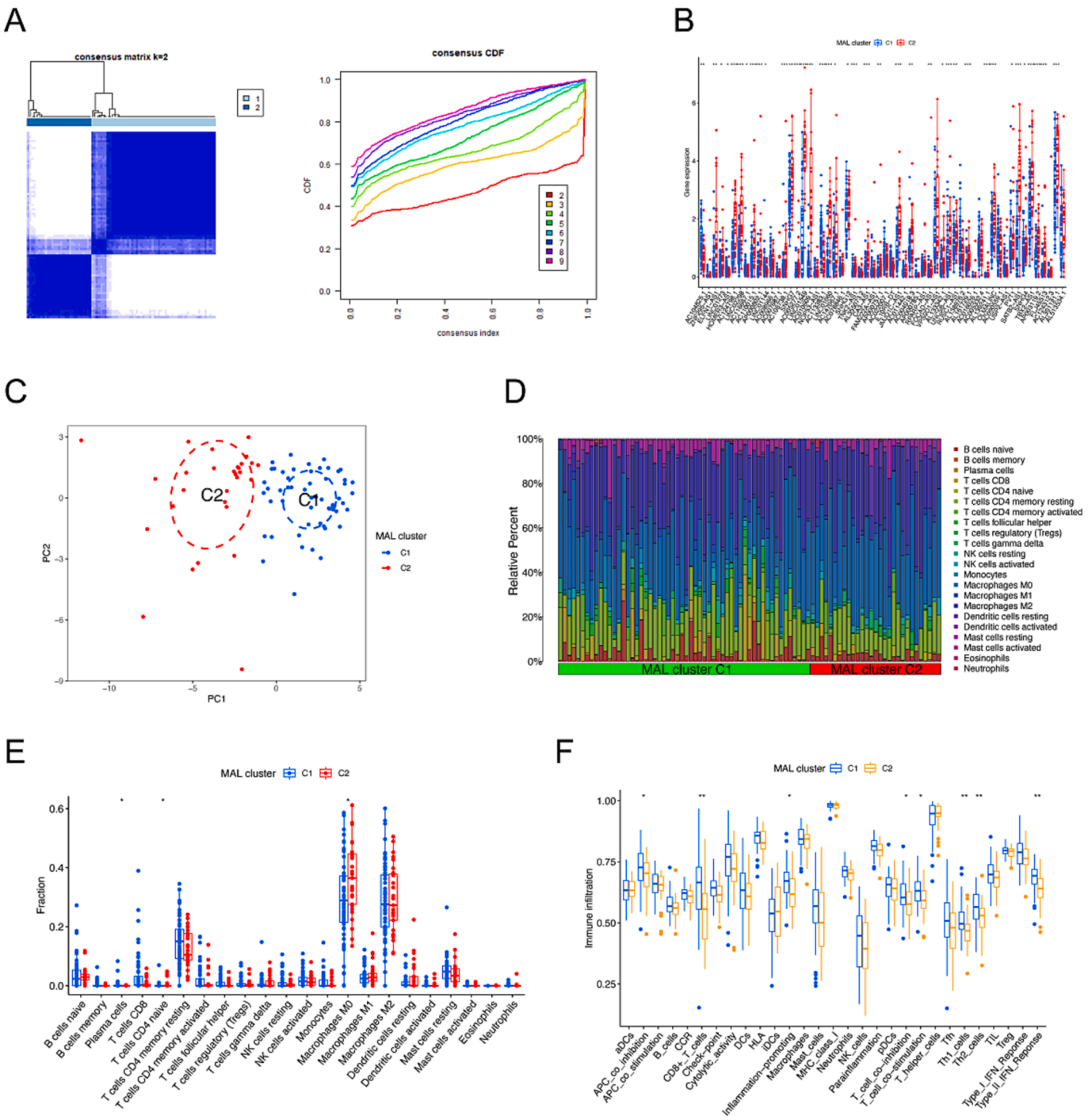

Fig. 4. Determination of MAL-related patterns in osteosarcoma by consensus clustering (A) Two MAL clusters were identified by consistent clustering analysis (k = 2). (B) The discrepancies in the abundance of MALs between the two clusters. (C) PCA analysis for two MAL patterns. (D) Heatmap of the 22 immune cell proportions in two MAL patterns by CIBERSORT analysis. (E) The distinction in 22 immune cell proportions between the two MAL clusters. (F) Comparison of immune cells and pathways in diverse MAL clusters by ssGSEA algorithm. MAL, mitochondria-related lncRNA; *p < 0.05; **p < 0.01; ***p < 0.001.

analysis revealed the heterogeneity of MAL patterns and effective differentiation of patients (Fig. 4C). The crosstalk between tumor cells and their surrounding TME is fundamental to tumorigenesis and progression [60]. We managed to quantify the TME cell infiltration profile and immune landscape disparities between the two MAL patterns by three different algorithms. The overall information on the content of 22 immune cells in two molecular subtypes is presented in Fig. 4D, where the abundance of M0 macrophages, plasma cells, and naive CD4 + T cells varied significantly from each other according to the CIBERSORT method (Fig. 4E). Meanwhile, the ssGSEA scores of eight TME features were distinguished between MAL patterns. APC co-inhibition, promoting inflammation, T cell co-inhibition, T cell co-stimulation, CD8 + T cells, Th1 cells, Th2 cells, and Type II IFN response pathways were activated in cluster C1 (Fig. 4F). In the ESTIMATE analysis, the two MAL clusters differed significantly in tumor purity, ESTIMATE, and stromal scores (Fig. 5A). In addition, we examined the relative expression of ICGs between MAL clusters C1 and C2. BTLA, LAIR1, CD200R1, CD40LG, VTCN1, PDCD1LG2, TNFRSF8, CD27, TNFRSF18, CD86, and CD44 were highly expressed in MAL cluster C1 samples, suggesting that MAL cluster C1 patients respond better to immunotherapy (Fig. 5B).

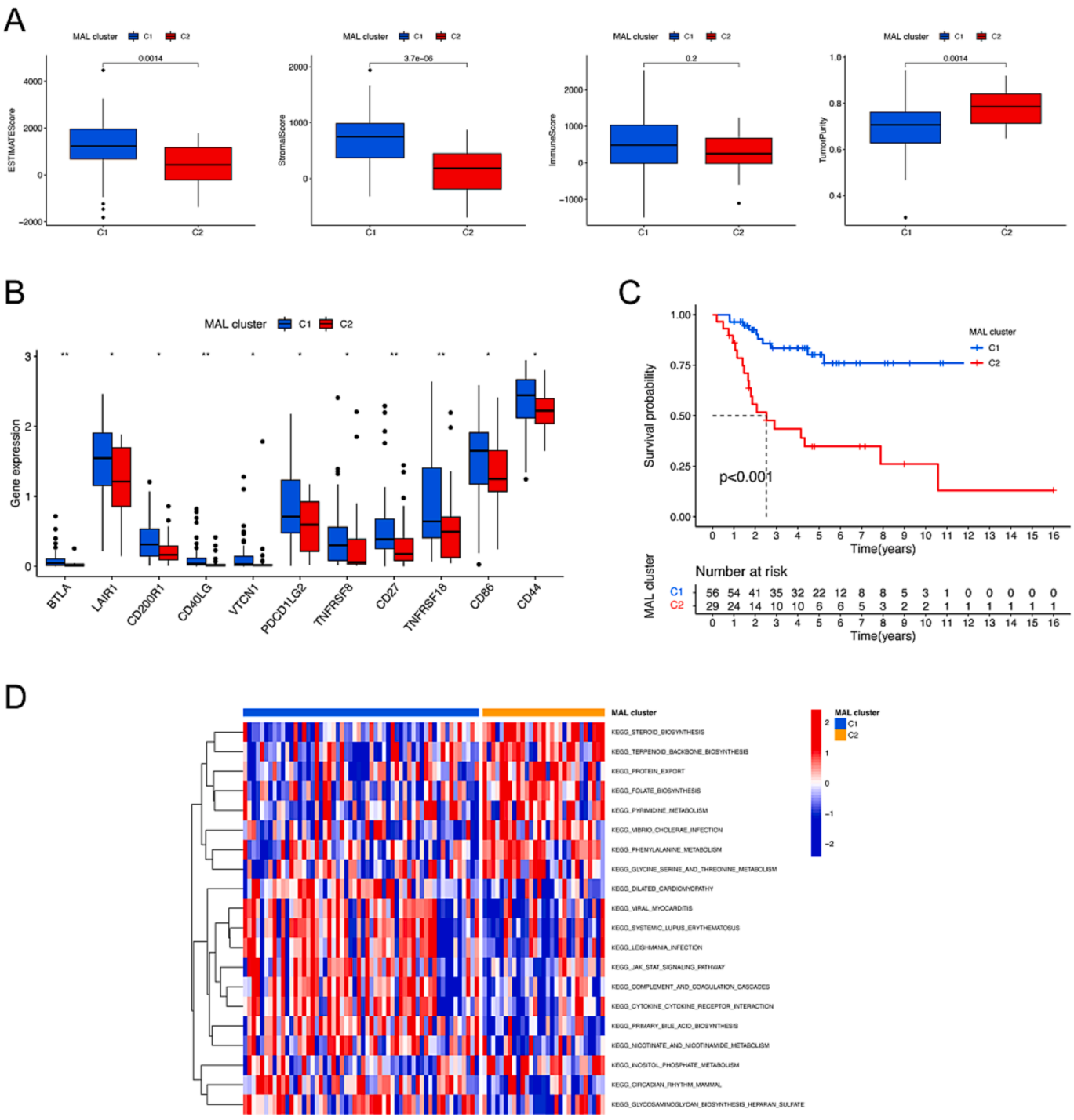

Fig. 5. ESTIMATE analysis, Kaplan-Meier survival analysis, and GSVA analysis for diverse MAL patterns (A) The distinction in ESTIMATE, stromal and immune scores, and tumor purity among diverse MAL patterns. (B) Discrepancies in immune checkpoint gene expression between diverse MAL patterns. (C) Kaplan-Meier survival curves of osteosarcoma patients with different MAL patterns. (D) GSVA enrichment analysis of osteosarcoma patients with different MAL patterns for ascertaining the activation status of biological pathways. MAL, mitochondria-related lncRNA; GSVA, gene set variation analysis; *p < 0.05; **p < 0.01.

Supportively, the clinical outcome analysis also showed that MAL cluster C2 had a better OS rate (Fig. 5C). To identify the underlying mechanisms contributing to the divergence between the two MAL patterns, we also conducted GSVA analysis. As shown in Fig. 5D, cluster C2 presented enriched pathways related to organic compound anabolism, such as steroid biosynthesis, terpenoid backbone biosynthesis, folate biosynthesis, pyrimidine metabolism, phenylalanine, glycine, serine, and threonine metabolism, compared to MAL cluster C1. These findings effectively demonstrate the validity and potential application of MAL-based clustering analysis in risk stratification of osteosarcoma patients.

3.4. Construction of the MAL scoring system

The MAL-based clustering analysis elucidated the general profile of MAL patterns in the osteosarcoma patient population, and the MAL scoring system was developed for application to specific individuals. After the LASSO regression of 58 prognostic MALs, six MALs were filtered for the construction of the MAL scoring system (Supplementary

Fig. S1). MAL scores = (ELFN1-AS1 * 0.350813) + (HOMER3-AS1 * −0.160669) + (LINC01549 * 0.055383) + (IL10RB-DT * −0.052315) + (AC011442.1 * 0.551401) + (AC090559.1 * −0.040253). Each osteosarcoma sample from the train, validation, or entire cohort was subjected to a MAL score and stratified into high- and low-MAL scoring groups (Fig. 6A–C). We observed that ELFN1-AS1, LINC01549, and AC011442.1 were enriched in the high MAL scoring group, while the opposite was true for HOMER3-AS1 (Fig. 6A–C). Survival analysis was then undertaken for these three cohorts. As shown in Fig. 6D–F, the patients with high-MAL scores presented discouraging results with higher mortality than those with low-MAL scores. ROC curve analysis reflected the accuracy of the MAL scoring system in the training cohort; with AUC greater than 0.85 for 1-, 3-, and 5-year OS (Fig. 6G). As expected, the ROC curve analysis for the test or entire cohort also suggested that the MAL score was a reliable prognostic indicator for osteosarcoma (Fig. 6H, I).

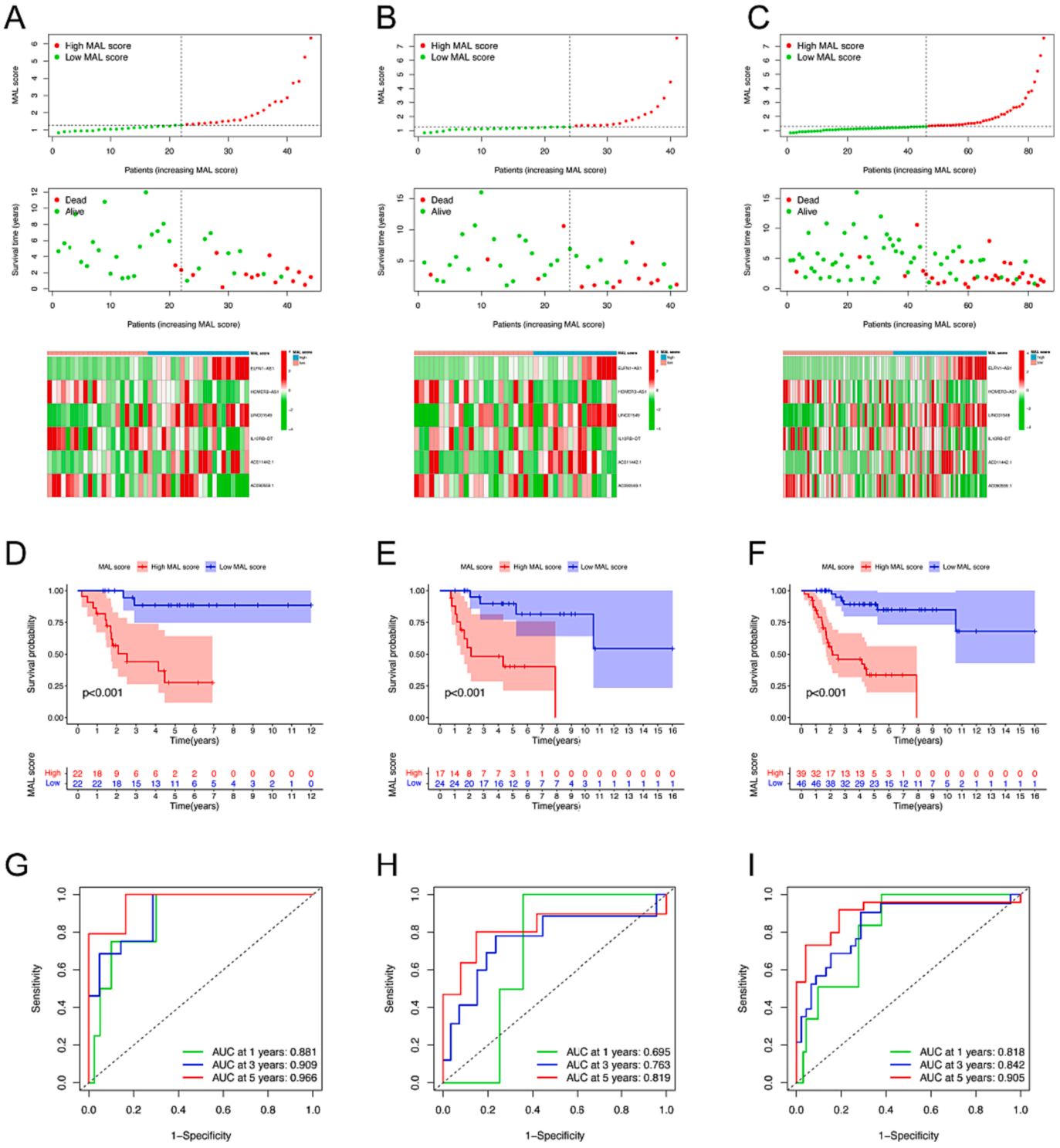

Fig. 6. Development and validation of the MAL scoring system (A-C) The MAL score distribution and MAL expression of osteosarcoma patients in the train (A) and validation (B), and entire (C) cohort. (D-F) Kaplan-Meier survival curves for osteosarcoma patients in the train (D) and validation (E), and entire (F) cohort. (G-I) ROC curves for 1-, 3-, and 5-year survival in train (G) and validation (H), and entire (I) cohort. MAL, mitochondria-related lncRNA.

3.5. Function annotation and clinical application of the MAL score

We also explored potential divergent mechanisms and activation pathways in patients with distinct MAL scores by GSEA analysis. Numerous crucial functions pertaining to immune development were significantly enhanced in the low MAL score subgroup, including activation of immune response, adaptive immune response, complement activation, humoral immune response, and phagocytosis, which may provide some evidence to substantiate the prognostic superiority of the low MAL score group (Fig. 7A). On the other hand, the pivotal enrichment functions in the elevated MAL score group were "diencephalon development", "intermediate filament organization", "muscle hypertrophy in response to stress", and others (Fig. 7B). Furthermore, the KEGG pathway specialized among the different scoring groups, with a prominently active hedgehog signaling pathway in the high MAL score group (Fig. 7C). In contrast, osteosarcoma patients with depressed MAL scores were more enriched with complement and coagulation cascades, hematopoietic cell lineage, and NOD-like receptor signaling pathway, among others (Fig. 7D).

The variation of clinicopathological parameters between the two

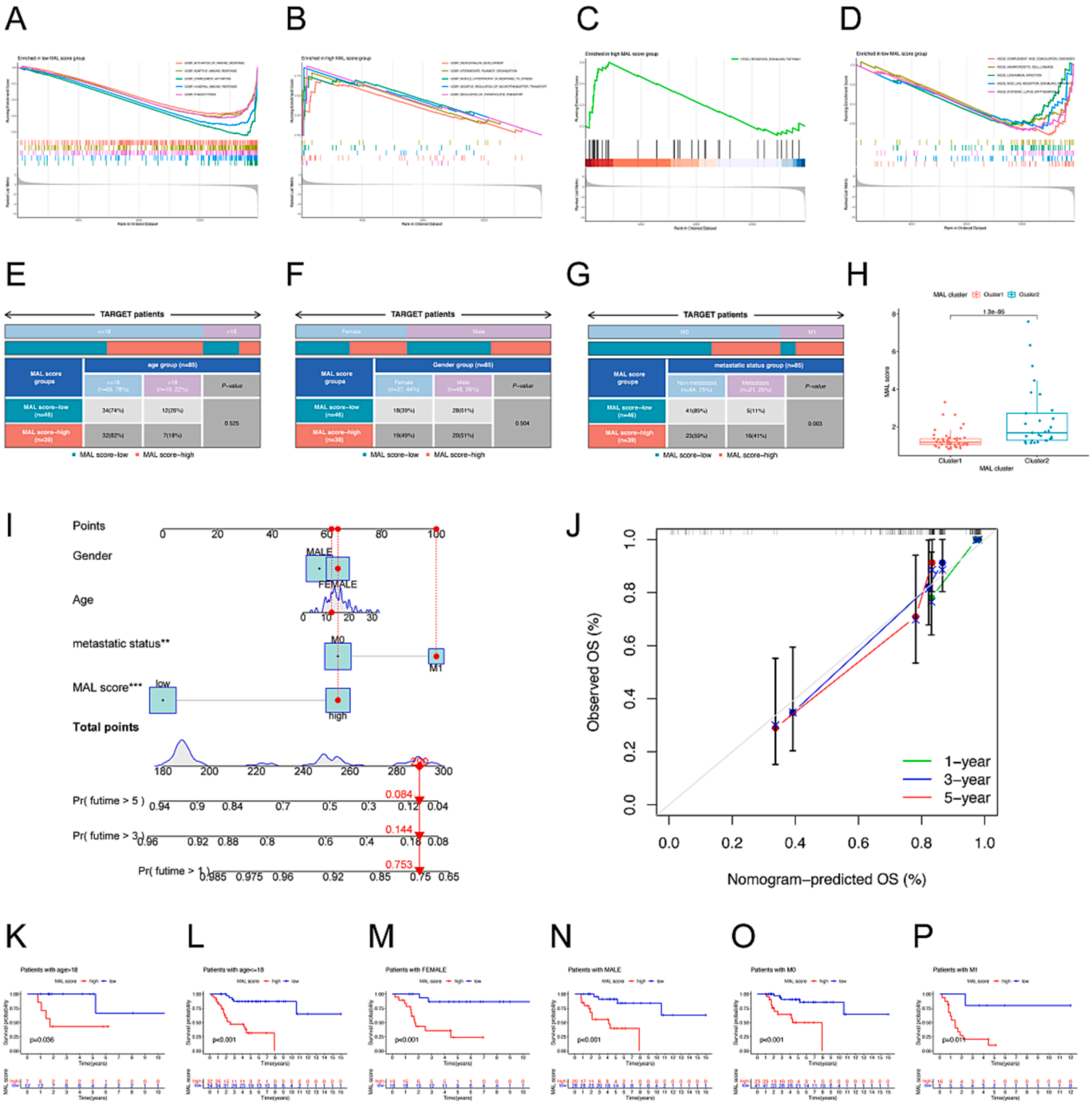

Fig. 7. MAL score-based functional annotation, clinical correlation analysis, and Nomogram construction (A-B) Gene Ontology enrichment in the low (A) and high (B) MAL score group by GSEA. (C-D) Kyoto Encyclopedia of Genes and Genomes enrichment in high (C) and low (D) MAL score group by GSEA. (E-G) Discrepancies in gender (E), age (F), and metastatic status (G) between different MAL score subgroups. (H) Discrepancies in MAL score between two MAL clusters. (I) Construction of a MAL-based nomogram by various parameters. (J) Calibration curve of the MAL-based nomogram. (K–P) Kaplan-Meier survival curves of overall survival stratified by age, gender, and metastasis status between low- and high-MAL score groups. MAL, mitochondria-related lncRNA; GSEA, Gene sets enrichment analysis.

MAL score groups was investigated. Notably, there were no significant disparities in age as well as gender between the diverse MAL score groups, but the probability of metastasis was higher in patients with high MAL scores (Fig. 7E–G). This suggests that the MAL score may be associated with metastasis in osteosarcoma. Interestingly, the risk score for cluster C1 was significantly lower than that for cluster C2 and corresponded to a better survival outcome, demonstrating that MAL patterns and scoring system could be mutually validated (Fig. 7H). We then created a nomogram combining MAL score and clinicopathological variables for osteosarcoma patients, allowing convenient prediction of OS at 1, 3, and 5 years (Fig. 7I). The conformity between the predicted and actual OS probabilities was assessed by calibration curves (Fig. 7J). In addition, stratified survival analysis revealed a greater survival discriminatory value of the MAL scoring system in multiple clinical subgroups including different age, gender, and metastasis groups, with significantly inferior OS in the high MAL score group (Fig. 7K–P).

3.6. Independent prognostic analysis and comparative evaluation of MAL scores

Cox regression was employed to appraise the independent prognostic value of MAL scores, and the results declared that metastasis status and MAL scores were independent prognostic elements in osteosarcoma patients with p-values < 0.05 (Fig. 8A, B). In estimating the prognosis of individual osteosarcoma patients, the AUC of the MAL scores was 0.905, which was superior to the clinical factors (Fig. 8C). The C-index was used to characterize the discriminatory ability of the MAL scores, which was likewise elevated over the clinical factors (Fig. 8D). To further confirm the distinguishability of the MAL scores, we carried out a ROC analysis of MAL scores versus four published prognostic models in the same osteosarcoma cohort and concluded that the AUC values of the MAL scores were not inferior to those of the other signatures (Fig. 8E).

3.7. MAL scores and tumor-infiltrating immune cells

For examining the impact of MAL scores on the immune landscape, TICs in distinct MAL score groups were first characterized using the ssGSEA algorithm. We uncovered that the TICs correlated with adaptive immunity were abundant in the low-MAL score group, including B cells, CD8 + T cells, T follicular helper (Tfh) cells, tumor-infiltrating lymphocytes (TIL), T helper type 1 cell (Th1 cells), Th2 cells, and regulatory T cells (Treg) (Fig. 9A). Meanwhile, APC co-inhibition, check point, cytolytic activity, inflammation − promoting, T cell co − inhibition, and co − stimulation pathways were significantly enhanced in the low-MAL score group (Fig. 9B). The ESTIMATE algorithm revealed significant differences in immunological subtypes between MAL score groups, with increasing MAL scores accompanying elevated tumor purity, but the reverse for ESTIMATE score and stromal score (Fig. 9C). The CIBERSORT algorithm discerned that the MAL scores were significantly positively correlated with M0 macrophages ($R = 0.24$, $p = 0.026$), but negatively correlated with plasma cells ($R = -0.26$, $p = 0.016$), activated memory CD4 + T cells ($R = -0.22$, $p = 0.041$), and CD8 + T cells ($R = -0.23$, $p = 0.037$) (Fig. 9D). Intriguingly, among the six MALs, the expression of AC090559.1 manifested a strong positive correlation with infiltrated M2 macrophages. On the other hand, LINC01549 was inversely linked to the infiltration of three immune cells, including CD8

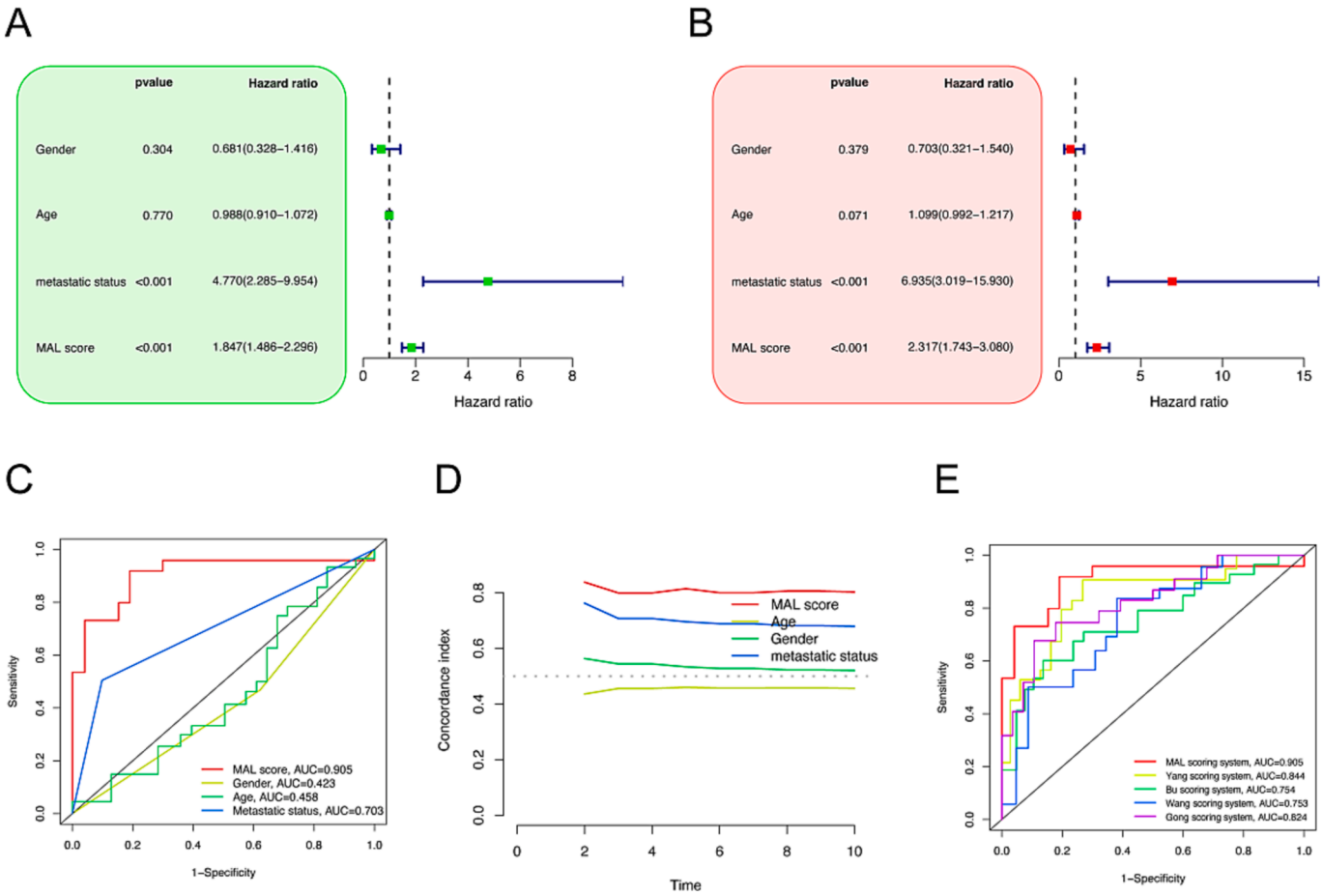

Fig. 8. Independent prognostic value and Comparative analysis of MAL scores (A-B) Univariate (A) and multivariate (B) independent prognostic analysis of MAL score and clinical variables. (C) Comparison of the predictive performance of MAL score and different clinical features by ROC analysis. (D) Comparison of the C-index between MAL score and clinical variables. (E) Comparison of MAL score with published lncRNA scoring systems. MAL, mitochondria-related lncRNA.

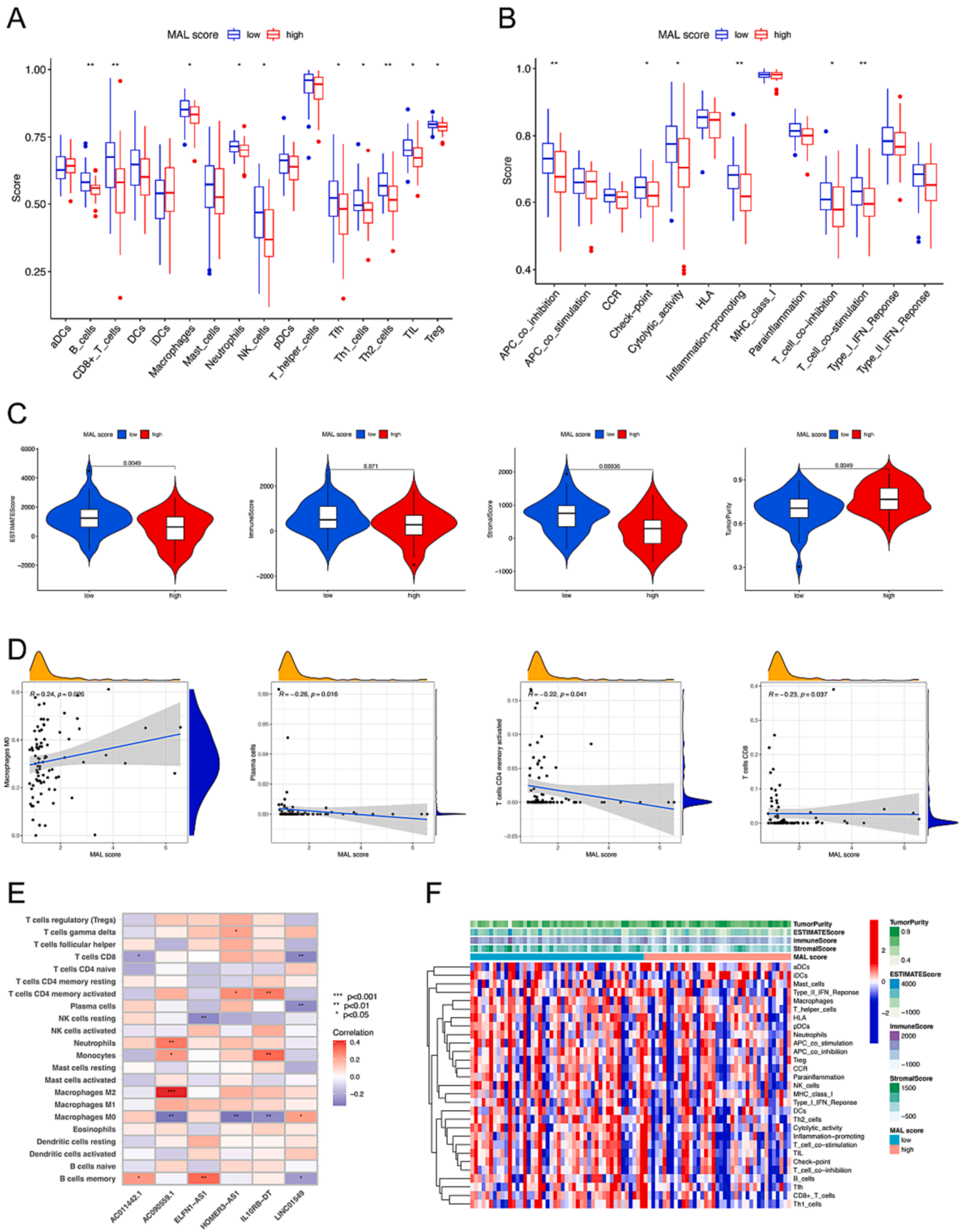

Fig. 9. Extended application of MAL score in the immune landscape (A-B) Comparison of immune cell infiltration and immune-related functions in diverse MAL score subgroups by single-sample gene-set enrichment analysis. (C) ESTIMATE analysis of diverse MAL score subgroups. (D) Correlation analysis between MAL score and immune infiltrating cells based on the CIBERSORT algorithm. (E) Correlation analysis between core MALs and immune infiltrating cells based on the CIBERSORT algorithm. (F) Heatmap for visualization of differences in the immune score, stromal score, ESTIMATE score, tumor purity, immune cells, and function in distinct MAL score subgroups. MAL, mitochondria-related lncRNA; *p < 0.05; **p < 0.01; ***p < 0.001.

+ T cells, plasma cells, and memory B cells (Fig. 9E). Fig. 9F details the distribution of MAL scores, immune functions, TICs, immune scores, stromal scores, ESTIMATE scores, and tumor purity among individual osteosarcoma patients. As expected, significant distinctions in the immune landscape were observed in the different MAL score groups, which is consistent with the prognostic analysis. These findings suggested that an activated immune status may account for better OS outcomes in the low-MAL score group.

3.8. ICB response metrics and drug sensitivity analysis

We calculated the IC50 values of several commonly prescribed targeted compounds and chemotherapeutic agents to further investigate the underlying merits of the MAL scoring system in clinical application. As described in Fig. 10A–I, bexarotene, bortezomib, docetaxel, gemcitabine, midostaurin, obatoclax mesylate, pazopanib, shikonin, and vinorelbine had lower IC50 values in the low MAL scoring group, indicating that low MAL score group was connected with a higher sensitivity to these agents. On the other hand, the relative likelihood of response to elesclomol, lenalidomide, methotrexate, pyrimethamine, sunitinib, and thapsigargin was elevated in the high MAL scoring group (Fig. 10J–O). Immune checkpoint analysis demonstrated that BTLA, LAIR1, LAG3, CD200R1, TMIGD2, PDCD1LG2, TNFSF9, KIR3DL1, TNFSF14, CD27, CD48, HAVCR2, CD274, HHLA2, CD44, TNFRSF9, and CD40LG were downregulated in the low MAL scoring group, reflecting the potential greater clinical benefit of ICB implementation in the low MAL subgroup (Fig. 10P). In addition, 16 immune checkpoints (TNFSF15, BTLA, CD27, CD40LG, CD44, CD200R1, CD274, HHLA2, LAG3, LAIR1, LGALS9, PDCD1LG2, TMIGD2, TNFRSF9, TNFSF4, and HAVCR2) were all strongly negatively correlated with MAL score ($P < 0.05$, Supplementary Fig. S2). Structural and functional variation in HLA underlies an effective adaptive immune response to tumor antigens, with individual variation in HLA genotype patterns potentially affecting the clinical outcome of ICB therapy [61,62]. Increased expressions of HLA class I genes (including HLA − A, HLA − E, and HLA − B) and HLA class II genes (including HLA − DMA, HLA − DMB, HLA − DPA1, HLA − DQA2, HLA − DQB1, HLA − DRB1, and HLA − DRB6) were observed to be associated with low MAL scores ($P < 0.05$, Supplementary Fig. S3). Our results indicated that patients in different scoring groups have divergent immunogenomic patterns and may be differentiated between immunotherapy responders and non-responders based on the MAL scoring system.

3.9. lncRNA-mRNA network, immunofluorescence localization and 3D structure prediction of MRGs

Based on Pearson correlation ($|R| > 0.4$ and $p < 0.001$), a lncRNA-mRNA co-expression network involving six MALs of the scoring system was created using Cytoscape (Fig. 11A). ELFN1-AS1 was co-expressed with HPDL, and HOMER3-AS1 was co-expressed with LYRM1. LINC01549 was co-expressed with 2 MRGs (AADAT and ETFBKMT), while IL10RB-DT was co-expressed with 3 MRGs (ALDH4A1, MLYCD, and ADCK1). AC011442.1 was co-expressed with ADCY10, and AC090559.1 was co-expressed with ABCB6. As shown in Fig. 11B–J, 3D protein structure predictions were applied for the nine MRGs mentioned above to facilitate the understanding of their functions. Based on the HPA database, the subcellular localization of HPDL, LYRM1, AADAT, ADCK1, and ABCB6 in U2OS was acquired using nucleus, microtubule, and endoplasmic reticulum (ER) markers. In U2OS cells, AADAT localized not only to the plasma membrane but also to the vesicles (Fig. 11*K*). ABCB6 and HPDL were primarily located in mitochondria (Fig. 11*L*, M), while ADCK1 and LYRM1 were mainly localized in the nucleoplasm (Fig. 11N, O).

3.10. Pan-cancer analysis of core MALs

As pan-cancer analysis of the six MALs in the scoring system has not been undertaken, it remains uncertain whether they conferred contribution to the pathogenesis of different tumors through specific or common molecular mechanisms. We executed pan-cancer analysis to investigate biomarkers suitable for broad-spectrum cancer diagnosis.

Comparative analysis of the MAL expression in pan-cancer and normal tissues revealed that ELFN1-AS1 was differentially expressed in 14 cancers and upregulated in 11 of them, including rectum adenocarcinoma (READ), stomach adenocarcinoma (STAD), colon adenocarcinoma (COAD), head and neck squamous cell carcinoma (HNSC), liver hepatocellular carcinoma (LIHC), lung adenocarcinoma (LUAD), bladder urothelial carcinoma (BLCA), breast invasive carcinoma (BRCA), lung squamous cell carcinoma (LUSC), prostate adenocarcinoma (PRAD), and uterine corpus endometrial carcinoma (UCEC) (Fig. 12A). HOMER3-AS1 was highly expressed in the majority of cancers, such as BLCA, cholangiocarcinoma (CHOL), esophageal carcinoma (ESCA), STAD, glioblastoma multiforme (GBM), HNSC, kidney renal clear cell carcinoma (KIRC), kidney renal papillary cell carcinoma (KIRP), LIHC, and LUSC, and was decreased in COAD, kidney chromophobe (KICH), and thyroid carcinoma (THCA) (Fig. 12B). LINC01549 expression levels were detectable but low in most tumors and adjacent normal tissues, with no significant discrepancies between BLCA, CHOL, ESCA, GBM, HNSC, KIRP, THCA, and matched normal tissues (Fig. 12C). IL10RB-DT was upregulated in 10 cancers and downregulated in 4 cancers compared to normal tissues (Fig. 12D). AC090559.1 was decreased in most cancers, including BLCA, BRCA, COAD, KIRP, LIHC, LUAD, LUSC, PRAD, READ, and UCEC (Fig. 12E). The expression level of AC011442.1 was tumor specificity, with relatively elevated expression in BLCA, CHOL, ESCA, KIRC, LIHC, LUAD, PRAD, STAD, and THCA, and relatively reduced expression in BRCA, HNSC, and KICH (Fig. 12F).

Survival analysis of the pan-cancer cohort demonstrated that ELFN1-AS1 expression affected OS in patients with adrenocortical carcinoma (ACC), COAD, KIRC, KIRP, acute myeloid leukemia (LAML), PAAD, UCEC, and uveal melanoma (UVM) and those patients with high levels of ELFN1-AS1 expression had a poorer prognosis than those with depressed levels of ELFN1-AS1 expression (Fig. 13A). KIRC and brain lower grade glioma (LGG) Patients with low AC011442.1 expression exhibited significantly increased OS, while HNSC patients with low AC011442.1 expression experienced inferior clinical outcomes (Fig. 13B). In ACC, KIRC, and UVM, patients with low IL10RB-DT expression levels had more favorable outcomes, but the converse occurred in BLCA, LUAD, and thymoma (THYM) (Fig. 13C). There were disparities in OS between patients with high and low LINC01549 expression in HNSC, KICH, KIRC, and uterine carcinosarcoma (UCS) (Fig. 13D). AC090559.1 expression was linked to prognosis in five cancers, namely ACC, LGG, LUAD, SKCM, and testicular germ cell tumors (TGCT) (Fig. 13E). Upregulated HOMER3-AS1 expression was substantially associated with unfavorable OS in KIRC, LIHC, and OV, but corresponded to better OS in BLCA and LAML (Fig. 13F).

Examination of cancer stemness highlighted six MALs with varying degrees of association with RNAss and DNAss in different cancer types (Fig. 14A, B). In general, AC090559.1 was negatively linked to RNAss or DNAss, with the strongest connection to RNAss in THYM ($r = -0.71$) (Fig. 14A, B, Supplementary Table S7). In opposition, ELFN1-AS1 was positively affiliated with RNAss in 12 cancers (including BRCA, cervical squamous cell carcinoma and endocervical adenocarcinoma (CESC), COAD, HNSC, LUAD, ovarian serous cystadenocarcinoma (OV), pancreatic adenocarcinoma (PAAD), PRAD, READ, skin cutaneous melanoma (SKCM), STAD, and UCEC), with the strongest association with RNAss in PAAD ($r = 0.44$) (Fig. 14A, Supplementary Table S7). Immunogenomic-based analysis identified six immune subtypes for defining differential immune response patterns affecting prognosis [63]. As illustrated in Fig. 14C, the six MALs were differentially expressed in the pan-cancer immune subtypes. Concretely, there was overexpression

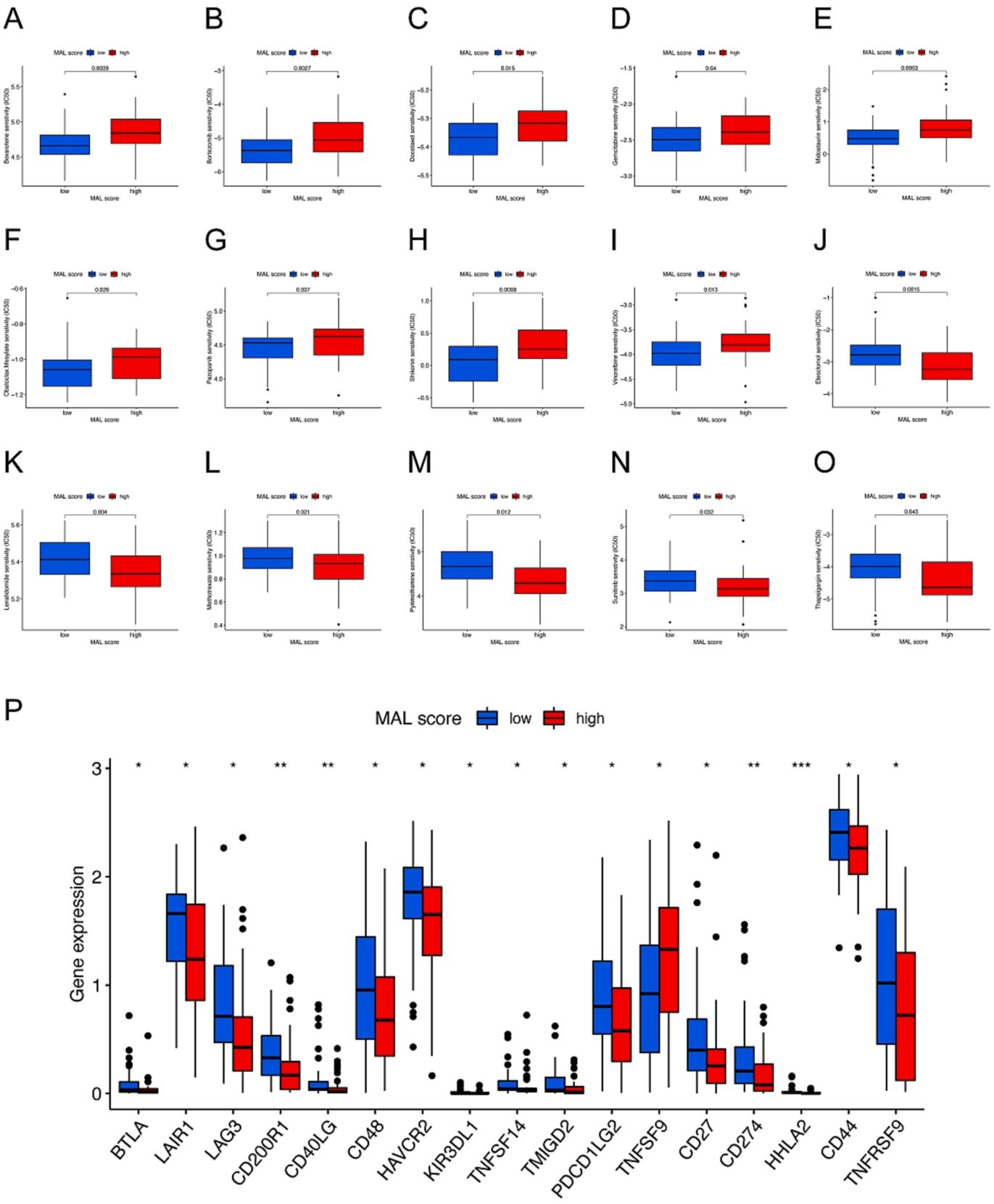

Fig. 10. Characteristics of MAL score in immune checkpoint expression and chemotherapy (A-O) Discrepancies in drug sensitivity between diverse MAL score subgroups, including bexarotene (A), bortezomib (B), docetaxel (C), gemcitabine (D), midostaurin (E), obatoclax.mesylate (F), pazopanib (G), shikonin (H), vinorelbine (I), elesclomol (J), lenalidomide (K), methotrexate (L), pyrimethamine (M), sunitinib (N), thapsigargin (O). (P) Discrepancies in immune checkpoint gene expression between diverse MAL score subgroups. MAL, mitochondria-related lncRNA.

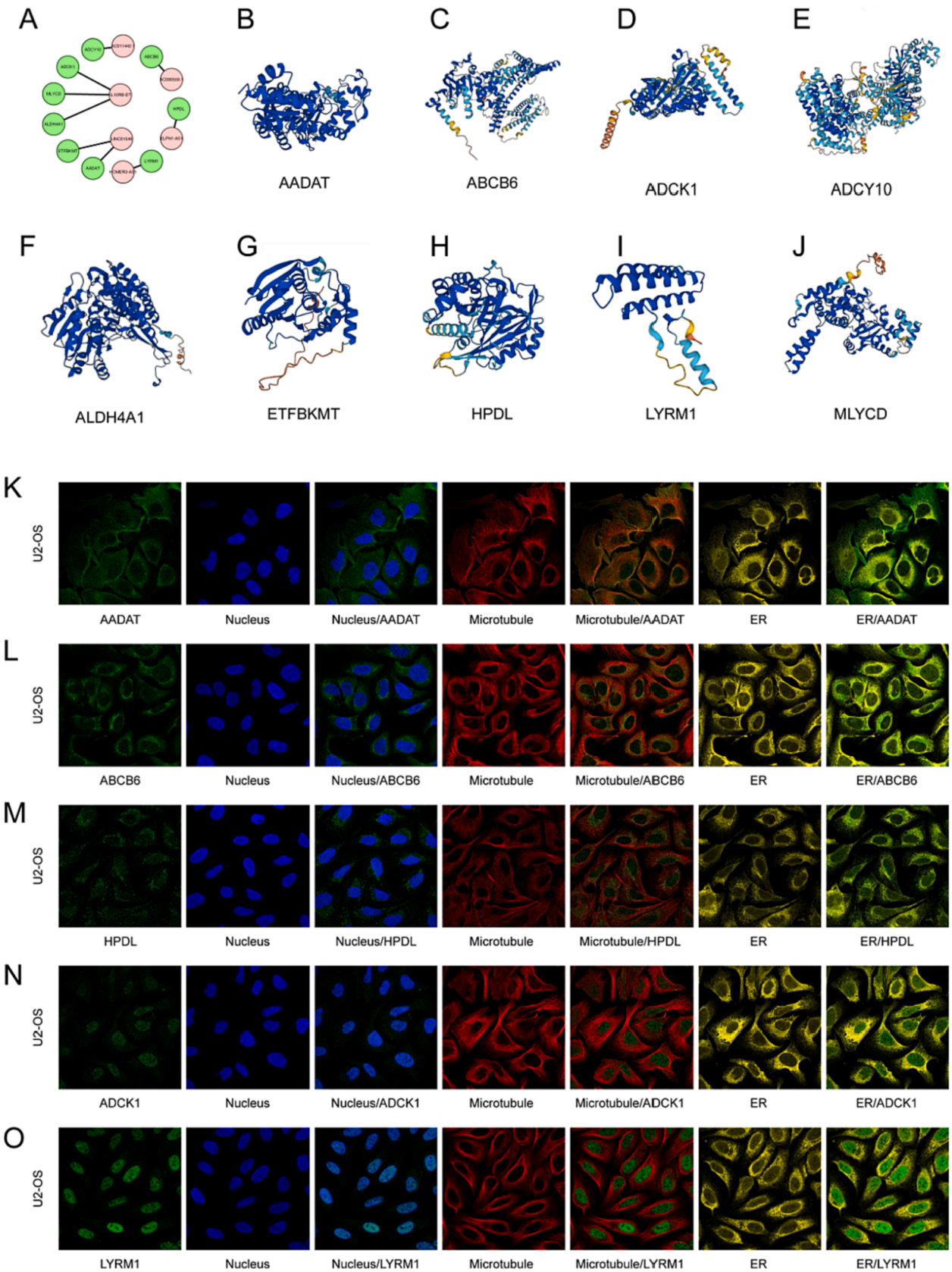

Fig. 11. Three-dimensional structure prediction and subcellular localization analysis of co-expressed MRGs (A) Network analysis of MALs with the nine most critically co-expressed MRGs. (B-J) Three-dimensional protein structure of nine most critically co-expressed MRGs. (K-O) Immunofluorescence staining of the subcellular localization of co-expressed MRGs, including AADAT, ABCB6, HPDL, ADCK1, and LYRM1. MAL, mitochondria-related lncRNA.

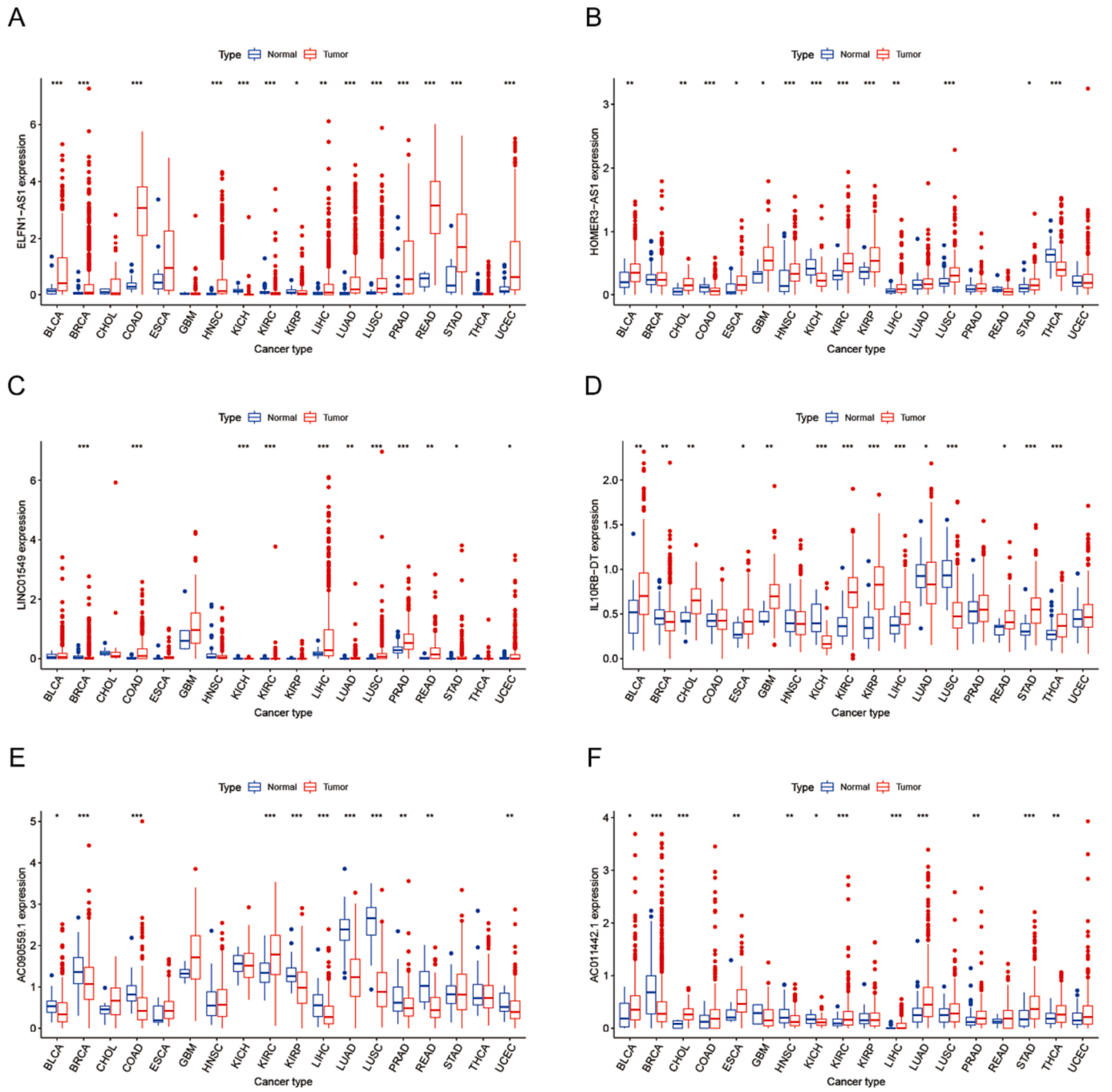

Fig. 12. Pan-cancer expression analysis of core MALs (A-F) Pan-cancer expression analysis of ELFN1-AS1 (A), HOMER3-AS1 (B), LINC01549 (C), IL10RB-DT (D), AC090559.1 (E), and AC011442.1 (F) in TCGA dataset. MAL, mitochondria-related lncRNA; *p < 0.05; **p < 0.01; ***p < 0.001.

of AC090559.1 and IL10RB-DT in the C6 immune subtype (TGF-beta dominant); ELFN1-AS1 and AC011442.1 in the C1 immune subtype (wound healing); and HOMER3-AS1 and LINC01549 in the C5 immune subtype (immunologically quiet).

In summary, the expression levels of the six MALs are dysregulated in multiple TCGA cancer types, with additional linkages to cancer prognosis, immune subtypes, and tumor stemness.

3.11. Subcellular localization and biological validation of core MALs

To further elucidate the possible mechanisms of core MALs, their subcellular localization was investigated using the lncATLAS database. HOMER3-AS1 was primarily localized in the nucleus (Fig. 15A). ELFN1-AS1 was mainly located in the cytoplasm of HUVEC and NCI.H460 cells and the nucleus of GM12878, HepG2, and K562 cells (Fig. 15B). IL10RB-DT was predominantly situated in the cytoplasm of GM12878 and SK.N.SH cells, as well as in the nucleus of HeLa.S3 and MCF.7 cells (Fig. 15C). The results of qRT-PCR further disclosed that the expression of ELFN1-AS1 and AC011442.1 was higher in all three osteosarcoma cell lines than in hFOB1.19 (Fig. 15D, E). In contrast, HOMER3-AS1 and IL10RB-DT were expressed inferiorly in osteosarcoma than in the human osteoblast cells (Fig. 15F, G). AC090559.1 was expressed higher in U2OS and MG63 cell lines, but not significantly different in the MNNG/HOS cells compared to the hFOB1.19 (Fig. 15H). Note that the CT values for LINC01549 were too high out of the RT-qPCR detection limit in hFOB1.19 and osteosarcoma cells, denoting a paucity of its

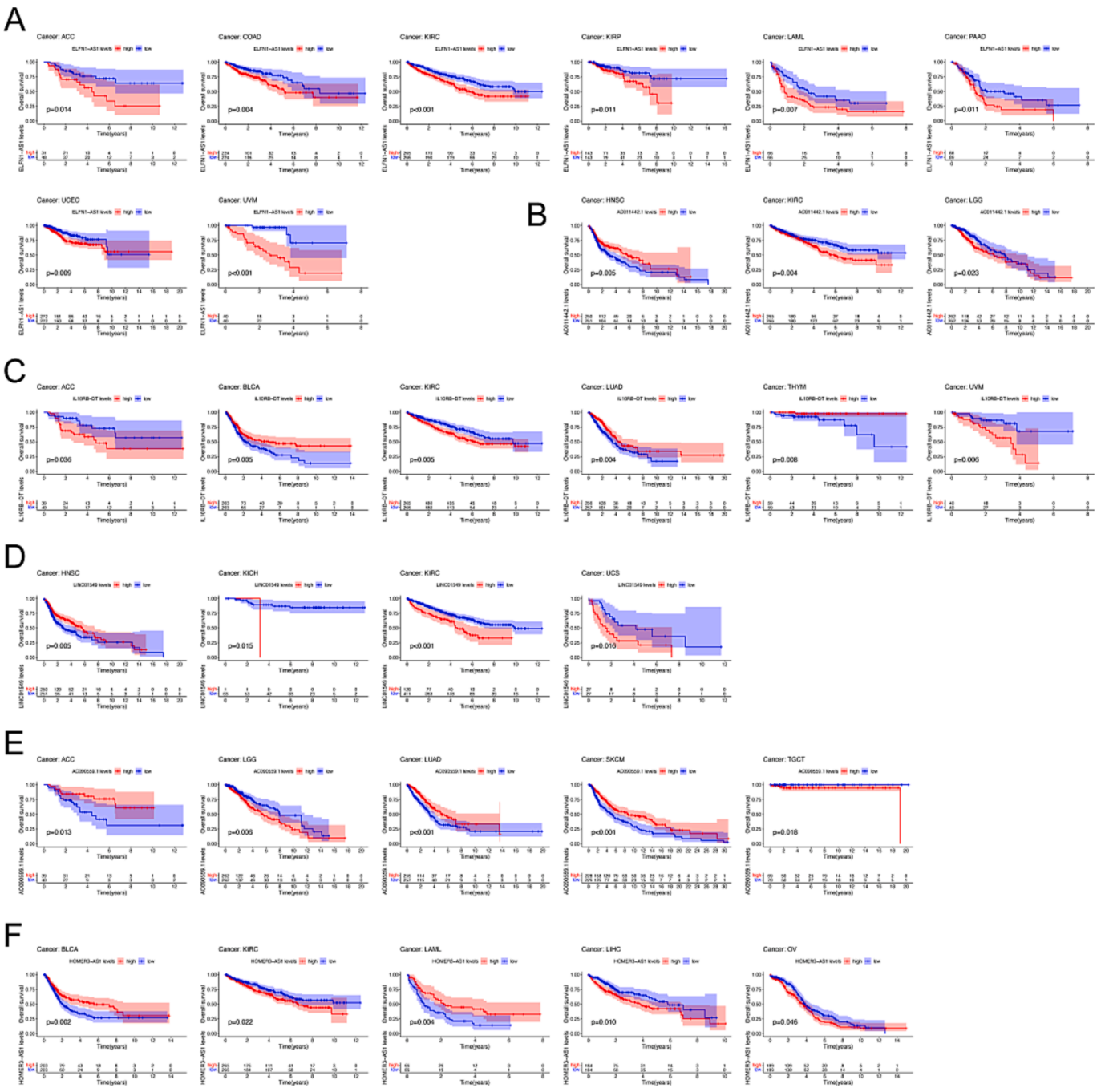

Fig. 13. Pan-cancer survival analysis of core MALs (A-F) Pan-cancer survival analysis of ELFN1-AS1 (A), HOMER3-AS1 (B), LINC01549 (C), IL10RB-DT (D), AC090559.1 (E), and AC011442.1 (F) in TCGA dataset. MAL, mitochondria-related lncRNA.

corresponding transcripts. Similarly in the pan-cancer analysis, we observed that LINC01549 exhibited extremely poor expression in various tumor and control samples (Fig. 12C).

4. Discussion

Osteosarcoma is the most common primary malignant bone cancer with severe morbidity and mortality [64,65]. The pathogenetic features of osteosarcoma are diverse and complex, including karyotypic instability, genomic disorders, disability of DNA restoration, DNA methylation, histone modifications, and immune escape [66,67]. The current therapeutic strategies were not ideal, especially for patients with advanced osteosarcoma and metastatic events [68]. Thus, further investigation of the underlying mechanisms from a new perspective and seeking effective systematic therapies to improve patients' prognoses is warranted. Recently, lncRNA signatures of various metabolic, programmed cell death and methylation modifications in osteosarcoma have been established. Given the lack of systematic analysis for crosstalk between MAL and the osteosarcoma microenvironment and prognosis, we performed a comprehensive assessment of MAL and co-expressed MRG using multi-omics data.

In this study, we first selected 32 crucial MRGs based on their expression levels and prognostic impact on patients with osteosarcoma, which have extensive interconnections. Further functional enrichment analysis revealed that as expected MRGs were enriched in substance metabolism, mitochondrial composition, and oxidative stress-related

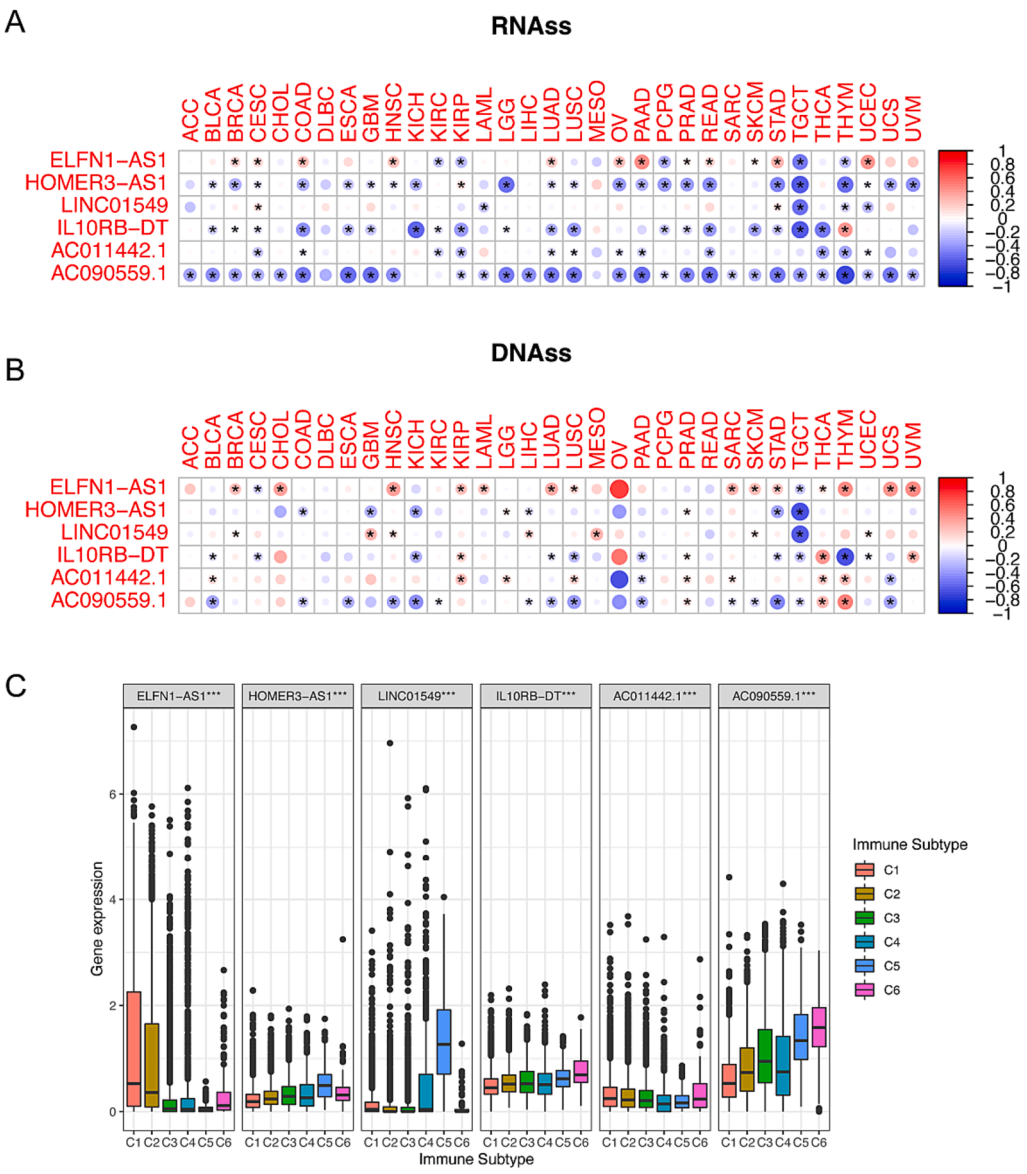

Fig. 14. Relationship of core MALs with immune subtype and tumor stemness score in pan-cancer (A) The correlation of core MALs expression with RNA stemness score. (B) The correlation of core MALs expression with DNA stemness score. (C) Differential expression of core MALs in six pan-cancer immune subtypes. MAL, mitochondria-related lncRNA; *p < 0.05; **p < 0.01; ***p < 0.001.

pathways. Reprogrammed metabolic demands and altered energy metabolism are crucial hallmarks of cancer, and mitochondria are the predominant organelles modulating cellular anabolism and signaling [69,70]. Cell fate is heavily implicated by mitochondrial activity, from ATP production to lipid metabolism, Ca2 + homeostasis, apoptosis, and oxygen radical stabilization [71]. Mitochondria within carcinoma cells tend to overproduce ROS, leading to a vicious cycle between mitochondria, ROS, genomic instability, and cancer progression [72]. These central MRGs may be potential molecular targets for revealing mitochondrial function in osteosarcoma, and further validation of their utility would be a bold and promising attempt.

To our knowledge, there is a surprising link between mitochondria and epigenetic regulation in cancer, as mitochondria could achieve modulation of epigenetics through cellular metabolites or Warburg effects [73]. Targeting epigenetics and mitochondrial metabolism has been proven as prospective therapeutic strategies to restrain tumor growth, which typically demonstrates synergistic benefits in conjunction with classical cytotoxic agents [73–75]. In turn, non-coding RNAs likewise serve indispensable components as in mediating cellular ROS release, mitochondrial function, and metabolic reprogramming [76]. Since lncRNAs affect oxidative stress and mitochondrial function through multiple mechanisms, which may have distinct effects on specific neoplastic phenotypes. Liu et al. reported that lncRNA ANRIL, an oncogenic factor upregulated in hepatocellular carcinoma, led to enhanced mitochondrial function and cell proliferation by driving increased ARL2 expression in a miR-199a-5p-dependent manner [77]. In another study, the hypoxia-induced elevation of LINC00294 could trigger the cAMP signaling pathway, depress mitochondrial function, and accelerate apoptosis in glioma cells through direct interaction with miR-21-5p, whereas silencing LINC00294 reversed mitochondrial dysfunction [78]. As part of our investigation, Pearson correlation analysis and univariate Cox regression were employed to recognize the 58 MALs with significant impact on the outcome of osteosarcoma patients from the TARGET dataset. In the following, two MAL subtypes were ascertained by unsupervised clustering and presented notable distinctions in patient survival time, immune characteristics, ICG abundance, and biological pathways. Specifically, each subtype showed separate enrichment patterns of mitochondrial function-related

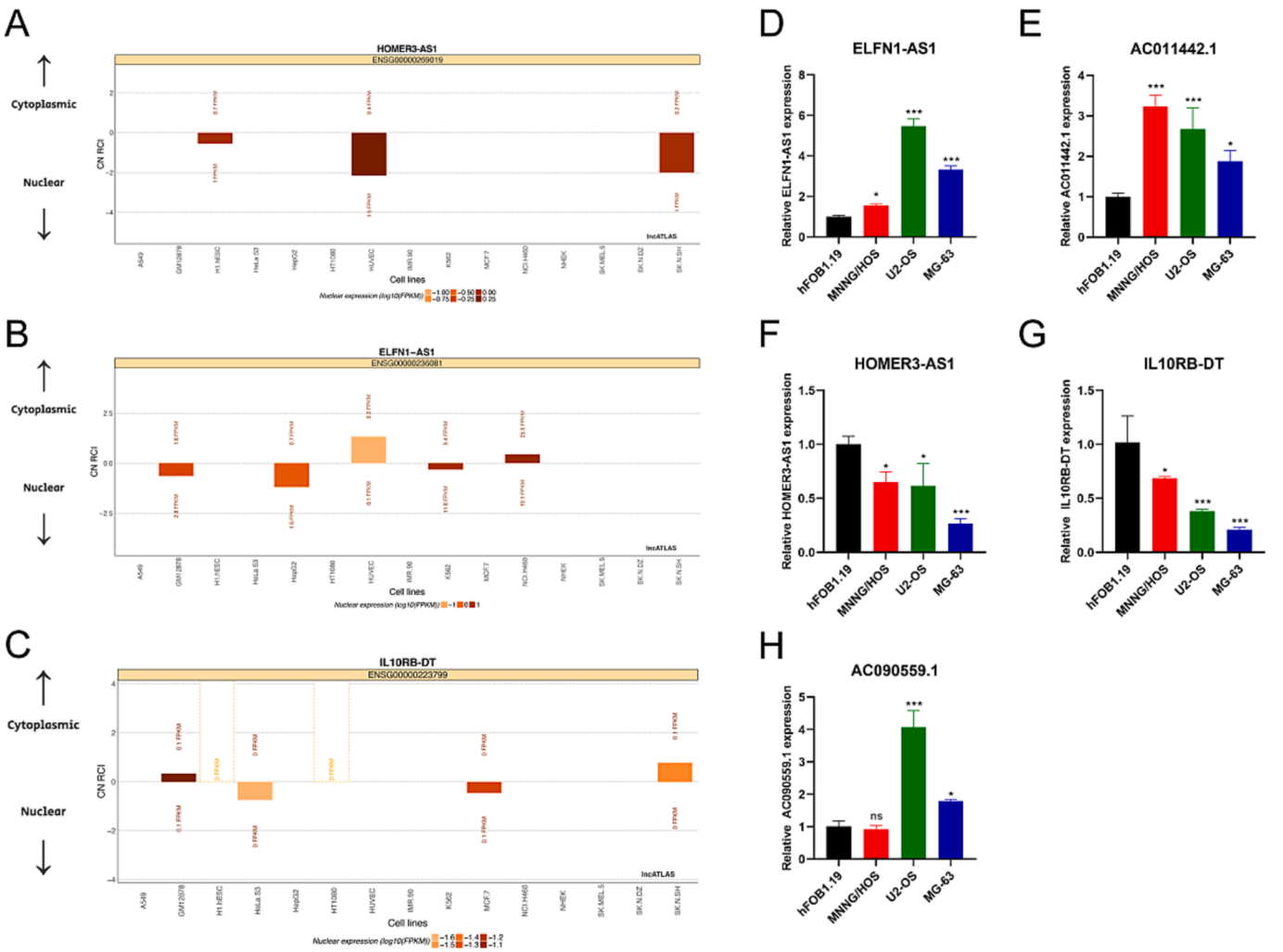

Fig. 15. Subcellular localization and expression levels of core MALs (A) The Subcellular localization of HOMER3-AS1 in the lncATLAS database. (B) The Subcellular localization of ELFN1-AS1 in the lncATLAS database. (C) The Subcellular localization of IL10RB-DT in the lncATLAS database. (D-H) The expression levels of ELFN1-AS1 (D), AC011442.1 (E), HOMER3-AS1 (F), IL10RB-DT (G), and AC090559.1 (H) in osteosarcoma and hFOB1.19 cell lines. MAL, mitochondria-related lncRNA; *p < 0.05; **p < 0.01; ***p < 0.001.

features, with folate biosynthesis, pyrimidine metabolism, phenylalanine, glycine, serine, and threonine metabolism significantly active in cluster C2. The complex and dynamic interactions between tumor-infiltrating immune cells and TME are responsible for tumor progression, including tumor escape, invasion, metastasis, and resistance to immunotherapy [79]. We analyzed the TME and the content of 22 immune cells in two osteosarcoma populations, and cluster C1 had a higher immune infiltration status, ESTIMATE scores, stromal scores, and a lower tumor purity while corresponding to a good prognosis. Upon the immunological background of the tumor, the immune-desert phenotype is defined as the absence of immune cell infiltration in tumor parenchyma or stroma [80], and we speculate that cluster C2 may be classified as an immune-desert phenotype. Characteristic molecular typing using MALs as the basis could facilitate new insights into the connections between classification and outcome in osteosarcoma patients.

For individual osteosarcoma patients, we determined six risk MALs (ELFN1-AS1, HOMER3-AS1, LINC01549, IL10RB-DT, AC011442.1, and AC090559.1) by lasso-penalized Cox regression analysis to construct a MAL scoring system. ROC curves and C-index curves suggested that the MAL score was reliable (even more robust than other published prognostic signatures) and could accurately predict the clinical outcomes of patients with osteosarcoma. Our study also examined the correlation between MAL scores and clinical characteristics of osteosarcoma patients. The patients with high MAL scores had a higher probability of developing metastases, in line with their poor outlook. Importantly, multivariate regression analysis indicated that the MAL score could be an independent prognostic factor for patients with osteosarcoma. We further observed that cluster C2 with unfavorable survival status scored much higher than cluster C1, demonstrating that MAL patterns and scoring system mutually validated each other's survival results. Numerous cancer types suffer from a complicated interconnection between mitochondrial dysfunction and the immune microenvironment [81]. Tumor-infiltrated T cells manifested diminished mitochondrial capacity and quality, which is linked to the inhibition of T cell mitochondrial biosynthesis and oxidative metabolism caused by TME [82]. In addition, suppression of OXPHOS and lipid metabolism in Treg cells exacerbated mitochondrial dysfunction and mtDNA release, followed by shaping the immunosuppressive environment [83]. Converting the phenotypes of immune cells from anticancer to carcinogenic decreases the ROS levels in the TME enabling the maintenance of tumor expansion [76]. Overall, it was necessary to further evaluate the interaction between MAL scoring systems with the tumor microenvironment and immune response. Three different algorithms revealed that the immune microenvironment was more favorable in low-scoring patients than in high-scoring patients, as reflected by the abundance of TICs relevant to adaptive immunity along with the activation of immune pathways such

as check point, cytolytic activity, inflammation-promoting, T cell co-inhibition in the low MAL score group. Also, the MAL scores of individual osteosarcoma patients were negatively correlated with the level of CD4 + and CD8 + T lymphocyte infiltration. CD4 + and CD8 + T lymphocytes with specificity for tumor-associated antigens could trigger the body's immune response to mediate apoptosis and cancer regression through ACT immunotherapy [84]. In clinical trials for melanoma patients, chimeric antigen receptor (CAR) T-cell immunotherapy has demonstrated outstanding efficiency in inducing complete and durable regression of metastatic melanoma [85]. Wu et al. proposed superior progression-free survival and OS in osteosarcoma patients infused with more CD8 + TIL [86]. HER2-targeted CAR-T therapy inhibited tumor-initiating cells and sarcosphere formation capacity in osteosarcoma revealing promising antitumor activity [87]. On the other hand, with the advent of ICB agents, curative options for cancer patients have dramatically widened. We observed that the expression levels of immune checkpoints were generally increased in the low MAL score subgroup than in the high MAL score subgroup, implying that the efficacy of ICB therapy may be better in patients with lower MAL scores [88]. The evolution of drug resistance in cancer patients is a principal challenge for clinical management. Augmented mitochondrial biogenesis and its dynamic alterations facilitate the development of chemoresistance by mechanisms ranging from altered metabolism, maintenance of stem cell properties, induction of autophagy, and activation of anti-apoptotic pathways [89]. Currently, therapeutic strategies targeting mitochondrial dysfunction against chemoresistance are receiving widespread attention [90]. Our study also extended the utility of the MAL scoring system in predicting osteosarcomas' susceptibility to various drugs. The high- and low-MAL scoring groups presented strikingly divergent responses to several chemotherapeutic agents (Bexarotene, Docetaxel, Gemcitabine, Midostaurin, Shikonin, and Vinorelbine). Although some of them are newly developed, we could screen chemotherapeutic agents suitable for osteosarcoma patients to guide future clinical administration. Overall, we systematically examined the relationship between the MAL scoring system and TME, immune cell infiltration, drug sensitivity, and immunotherapy response, which may assist in the prognostic assessment and treatment determination in osteosarcoma. Indeed, obtaining more data from osteosarcoma patients with previous immunotherapy or chemotherapy will enable us to characterize the effectiveness of different therapies, which is the direction of our future research.

For these lncRNAs included in the MAL scoring system (ELFN1-AS1, HOMER3-AS1, LINC01549, IL10RB-DT, AC090559.1, and AC011442.1), it is still unclear whether they contribute to the pathogenesis of different tumors through specific or common molecular mechanisms, so we further investigated their research progress. ELFN1-AS1 has been proven to participate in tumorigenesis and development as an oncogenic driver in colorectal cancer, retinoblastoma, ovarian cancer, pancreatic cancer, non-small cell lung cancer, and others [91–95]. Ge et al. found that ELFN1-AS1 displayed markedly elevated levels in advanced osteosarcoma patients and osteosarcoma cells, while the malignant phenotypes of osteosarcoma were inhibited after knocking down ELFN1-AS1 [96]. Mechanistically, the osteosarcoma cell-derived exosome ELFN1-AS1 promoted M2 macrophage polarization by serving as ceRNA to upregulate CREB1 expression [96]. In our study, ELFN1-AS1 was overexpressed in MG63, U2OS, and MNNG/HOS, following previous reports. LINC01549 expression was exceedingly depressed in most tumors and adjacent normal tissues and correlated with OS in patients with HNSC, KICH, KIRC, and UCS. According to Wang et al. LINC01549 may be engaged in necroptosis as a negative prognostic element in osteosarcoma patients [97]. Similarly, our study demonstrated that LINC01549 was upregulated in the high-MAL scoring group, corresponding to inferior clinical outcomes. Moreover, LINC01549 was negatively correlated with tumor-infiltrating CD8 + T cells, plasma cells, and memory B cells in the TME of osteosarcoma. As the main immune cells against cancer, CD8 + cytotoxic T lymphocytes (CTL) gradually lose their function and differentiate into an exhausted condition due to immune tolerance and immunosuppressive mechanisms [98]. Depleted CD8 + TILs manifest diminished mitochondrial fitness and excessive mitochondrial ROS, a phenomenon particularly exacerbated in TME [99]. Therapeutic enhancement of mitochondrial mass and morphology may allow for improved TIL performance [100]. TIL-B and plasma cells situated in tumors or tumor-associated tertiary lymphoid structures probably exert an aggressive part in antitumor immunity, but their potential utility as agents or targets for cancer immunotherapy demands further elucidation [101]. In GBM tissue, IL10RB-DT was markedly upregulated than in normal brain tissue and was an adverse prognostic biomarker independent of other clinical factors [102]. Another study illustrated that IL10RB-DT was overexpressed in clear cell renal cell carcinoma, especially in advanced T stages [103]. Yang et al. proposed that IL10RB-DT inhibited tumor antigen presentation and induced CD8 + T-cell depletion to suppress tumor immune responses, which was strongly negatively associated with the clinical efficacy of ICB and survival in melanoma and breast cancer [104]. Consistent with the results of Zhang et al [105], we demonstrated that IL10RB-DT was downregulated in MG63, U2OS, and MNNG/HOS. Co-expression analysis predicts that IL10RB-D may interact with three MRGs (ALDH4A1, MLYCD, and ADCK1), so further investigation of its specific function is warranted. Transcriptome data analysis of AC011442.1 revealed that it was differentially expressed in 12 tumors and significantly correlated with OS in patients with HNSC, KIRC, and LGG. According to Yi et al. AC011442.1 may act as an oncogenic driver in osteosarcoma regulating AMPK and hedgehog signaling pathways [106]. We investigated that AC011442.1 was highly expressed in high-MAL scoring subgroups and upregulated in MG63, U2OS, and MNNG/HOS. Notably, AC011442.1 has not been reported to be associated with biological functions in osteosarcoma, and its molecular mechanisms in osteosarcoma deserve additional characterization.AC090559.1 reportedly participated in the construction of ferroptosis, autophagy, and Pyroptosis-related prognostic models in LUAD, as well as serving as an independent favorable prognostic factor for OS [107–109]. Concordant with the published literature, LUAD patients with advanced levels of AC090559.1 expression had a more favorable outcome by pan-cancer analysis. Tumor progression is characterized by progressive loss of the differentiated phenotype and acquisition of stem cell-like features. Stem cell indices help stratify undifferentiated cancers, and assessment of tumor stemness based on RNA expression and DNA methylation characteristics is widely available [110]. Examination of cancer stemness suggested that AC090559.1 was adversely correlated with RNAss in most tumors, underscoring the necessity for further exploration of potential mechanisms. The tumor-promoting properties of HOMER3-AS1 have been adequately characterized in hepatocellular carcinoma, where HOMER3-AS1 upregulates CSF-1 and activates Wnt/β-catenin signaling to promote the malignant phenotype, while concurrently inducing macrophage recruitment and M2-like polarization [111]. Our study disclosed that HOMER3-AS1 negatively correlated with M0 macrophage infiltration in the TME of osteosarcoma and positively correlated with activated memory CD4 + T cells and gamma delta T cells. Multiple investigations have demonstrated that gamma delta T cells could directly target tumor cells through granule extravasation pathways, antibody-dependent cytotoxic effects, and secreted cytokines, as well as indirectly affect antitumor immunity by activating other immune cells and coordinating downstream immune responses [112,113]. M0 macrophages are precursors of polarized macrophages, while M2-polarized tumor-associated macrophages have pronounced tumor-promoting and immunosuppressive effects [114,115]. In contrast, classically activated macrophages with the M1 phenotype participate in antitumor immune responses by presenting antigens to adaptive immune cells [116]. Taken together, the six core MALs constituting this scoring system may be influential in tumor progression and prognosis, providing a reliable basis for further experiments.

However, there are some unavoidable limitations. First, due to the

insufficient sample size and retrospective character of the osteosarcoma cohort, the MAL scoring system still remains to undergo evaluation in various clinical cohorts (including prospective cohorts) to ensure its robustness. Second, more data on osteosarcoma patients who have received immunotherapy need to be mined in the future to analyze the exact relationship between the MAL score and immune response. In addition, further experiments are warranted to understand the detailed functional mechanisms of MALs.

5. Conclusion

In this research, we probed more accurate molecular phenotypes and systematically evaluated the value of MALs in predicting survival, TME cell infiltration, and response to immunotherapy and chemotherapy, which helped us in clinical stratification management.

Author contributions

YZ and NR conceived the research. YZ, NR, and ZX contributed to the data collection and interpretation. YZ, NR, WG, RP, ZW, and ZC conducted the experiments and administration. YZ and NR drafted the manuscript. HW and XZ critically revised the manuscript. All authors have read and agreed to the published version of the manuscript.

Declaration of Competing Interest

The authors declare that they have no known competing financial interests or personal relationships that could have appeared to influence the work reported in this paper.

Acknowledgments

This study was supported by the Medical Scientific Research Foundation of Guangdong Province (A2018544), the Science and Technology Projects in Guangzhou (202201020566, 2023A03J1015, 202201020087), the Research Fund Program of Guangdong Provincial Key Laboratory of Speed Capability Research, the National Natural Science Foundation of China (82074511, 82374558, 81973660), and the Clinical Frontier Technology Program of the First Affiliated Hospital of Jinan University, China (No. JNU1AF-CFTP-2022-a01204). The authors are very grateful to Rong He and Home for Researchers (www.home-for-researchers.com) for providing writing assistance.

Appendix A. Supplementary data

Supplementary data to this article can be found online at https://doi.org/10.1016/j.jbo.2023.100506.

References

[1] P. Chaiyawat, J. Settakorn, A. Sangsin, P. Teeyakasem, J. Klangjorhor, A. Soongkhaw, D. Pruksakorn, Exploring targeted therapy of osteosarcoma using proteomics data, OncoTargets Therapy 10 (2017) 565–577.
[2] C. Jacques, R. Tesfaye, M. Lavaud, S. Georges, M. Baud'huin, F. Lamoureux, B. Ory, Implication of the p53-Related miR-34c, -125b, and -203 in the osteoblastic differentiation and the malignant transformation of bone sarcomas, Cells 9 (4) (2020).
[3] S.S. Bielack, B. Kempf-Bielack, G. Delling, G.U. Exner, S. Flege, K. Helmke, R. Kotz, M. Salzer-Kuntschik, M. Werner, W. Winkelmann, A. Zoubek, H. Jürgens, K. Winkler, Prognostic factors in high-grade osteosarcoma of the extremities or trunk: an analysis of 1,702 patients treated on neoadjuvant cooperative osteosarcoma study group protocols, J. Clin. Oncol. 20 (3) (2002) 776–790.
[4] M.J. Klein, G.P. Siegal, Osteosarcoma: anatomic and histologic variants, Am. J. Clin. Pathol. 125 (4) (2006) 555–581.
[5] S. Yoshida, J. Celaire, C. Pace, C. Taylor, Y. Kaneuchi, S. Evans, A. Abudu, Delay in diagnosis of primary osteosarcoma of bone in children: Have we improved in the last 15 years and what is the impact of delay on diagnosis? J Bone Oncol 28 (2021), 100359.
[6] W. Wu, Y. Dai, H. Liu, R. Cheng, Q. Ni, T. Ye, W. Cui, Local release of gemcitabine via in situ UV-crosslinked lipid-strengthened hydrogel for inhibiting osteosarcoma, Drug Deliv. 25 (1) (2018) 1642–1651.
[7] O. Mitxelena-Iribarren, C.L. Hisey, M. Errazquin-Irigoyen, Y. González-Fernández, E. Imbuluzqueta, M. Mujika, M.J. Blanco-Prieto, S. Arana, Effectiveness of nanoencapsulated methotrexate against osteosarcoma cells: in vitro cytotoxicity under dynamic conditions, Biomed. Microdevices 19 (2) (2017) 35.
[8] M.S. Kim, S.Y. Lee, W.H. Cho, W.S. Song, J.S. Koh, J.A. Lee, J.Y. Yoo, D.S. Shin, D. G. Jeon, Prognostic effects of doctor-associated diagnostic delays in osteosarcoma, Arch. Orthop. Trauma Surg. 129 (10) (2009) 1421–1425.
[9] G.B. Andersen, A. Knudsen, H. Hager, L.L. Hansen, J. Tost, miRNA profiling identifies deregulated miRNAs associated with osteosarcoma development and time to metastasis in two large cohorts, Mol. Oncol. 12 (1) (2018) 114–131.
[10] A.L. Leichter, M.J. Sullivan, M.R. Eccles, A. Chatterjee, MicroRNA expression patterns and signalling pathways in the development and progression of childhood solid tumours, Mol. Cancer 16 (1) (2017) 15.
[11] J. Gu, Z. Zuo, L. Sun, L. Li, N. Zhao, Prognostic factors for laryngeal sarcoma and nomogram development for prediction: a retrospective study based on SEER database, Annals Trans. Med. 8 (8) (2020) 545.
[12] S. Wang, H. Li, S. Chen, Z. Wang, Y. Yao, T. Chen, Z. Ye, P. Lin, Andrographolide induces apoptosis in human osteosarcoma cells via the ROS/JNK pathway, Int. J. Oncol. 56 (6) (2020) 1417–1428.
[13] J. Klangjorhor, P. Chaiyawat, P. Teeyakasem, N. Sirikaew, A. Phanphaisarn, J. Settakorn, K. Lirdprapamongkol, S. Yama, J. Svasti, D. Pruksakorn, Mycophenolic acid is a drug with the potential to be repurposed for suppressing tumor growth and metastasis in osteosarcoma treatment, Int. J. Cancer 146 (12) (2020) 3397–3409.
[14] S.S. Ring, J. Cupovic, L. Onder, M. Lütge, C. Perez-Shibayama, C. Gil-Cruz, E. Scandella, A. De Martin, U. Mörbe, F. Hartmann, R. Wenger, M. Spiegl, A. Besse, W.V. Bonilla, F. Stemeseder, S. Schmidt, K.K. Orlinger, P. Krebs, B. Ludewig, L. Flatz, Viral vector-mediated reprogramming of the fibroblastic tumor stroma sustains curative melanoma treatment, Nat. Commun. 12 (1) (2021) 4734.
[15] D. Thomas, P. Radhakrishnan, Tumor-stromal crosstalk in pancreatic cancer and tissue fibrosis, Mol. Cancer 18 (1) (2019) 14.
[16] W. Wang, W. Zou, Amino acids and their transporters in t cell immunity and cancer therapy, Mol. Cell 80 (3) (2020) 384–395.
[17] A. Szewczyk, L. Wojtczak, Mitochondria as a pharmacological target, Pharmacol. Rev. 54 (1) (2002) 101–127.
[18] A.A. Parkhitko, E. Filine, S.E. Mohr, A. Moskalev, N. Perrimon, Targeting metabolic pathways for extension of lifespan and healthspan across multiple species, Ageing Res. Rev. 64 (2020), 101188.
[19] A. Kearns, J. Gordon, T.H. Burdo, X. Qin, HIV-1-Associated Atherosclerosis: Unraveling the Missing Link, J. Am. Coll. Cardiol. 69 (25) (2017) 3084–3098.
[20] C. Díaz de la Loza Mdel, M. Gallardo, M.L. García-Rubio, A. Izquierdo, E. Herrero, A. Aguilera, R.E. Wellinger, Zim17/Tim15 links mitochondrial iron-sulfur cluster biosynthesis to nuclear genome stability Nucleic acids research 39 14 2011 6002 6015.
[21] M.I. Whang, R.M. Tavares, D.I. Benjamin, M.G. Kattah, R. Advincula, D. K. Nomura, J. Debnath, B.A. Malynn, A. Ma, The ubiquitin binding protein tax1bp1 mediates autophagasome induction and the metabolic transition of activated t cells, Immunity 46 (3) (2017) 405–420.
[22] M. Salah, H. Akasaka, Y. Shimizu, K. Morita, Y. Nishimura, H. Kubota, H. Kawaguchi, T. Sogawa, N. Mukumoto, C. Ogino, R. Sasaki, Reactive oxygen species-inducing titanium peroxide nanoparticles as promising radiosensitizers for eliminating pancreatic cancer stem cells, J. Experimental Clin. Cancer Res.: CR 41 (1) (2022) 146.
[23] J. Li, L. Pan, W.G. Pembroke, J.E. Rexach, M.I. Godoy, M.C. Condro, A. G. Alvarado, M. Harteni, Y.W. Chen, L. Stiles, A.Y. Chen, I.B. Wanner, X. Yang, S. A. Goldman, D.H. Geschwind, H.I. Kornblum, Y. Zhang, Conservation and divergence of vulnerability and responses to stressors between human and mouse astrocytes, Nat. Commun. 12 (1) (2021) 3958.
[24] C.C. Xue, M.H. Li, Y. Zhao, J. Zhou, Y. Hu, K.Y. Cai, Y. Zhao, S.H. Yu, Z. Luo, Tumor microenvironment-activatable Fe-doxorubicin preloaded amorphous CaCO(3) nanoformulation triggers ferroptosis in target tumor cells, Sci. Adv. 6 (18) (2020) eaax1346.
[25] N. Verma, Y. Vinik, A. Saroha, N.U. Nair, E. Ruppin, G. Mills, T. Karn, V. Dubey, L. Khera, H. Raj, F. Maina, S. Lev, Synthetic lethal combination targeting BET uncovered intrinsic susceptibility of TNBC to ferroptosis, Sci. Adv. 6 (34) (2020).
[26] N. Kajarabille, G.O. Latunde-Dada, Programmed cell-death by ferroptosis: antioxidants as mitigators, Int. J. Mol. Sci. 20 (19) (2019).
[27] M.R. Ruocco, A. Avagliano, G. Granato, E. Vigliar, S. Masone, S. Montagnani, A. Arcucci, Metabolic flexibility in melanoma: a potential therapeutic target, Semin. Cancer Biol. 59 (2019) 187–207.
[28] S. Toki, T. Yoshimaru, Y. Matsushita, H. Aihara, M. Ono, K. Tsuneyama, K. Sairyo, T. Katagiri, The survival and proliferation of osteosarcoma cells are dependent on the mitochondrial BIG3-PHB2 complex formation, Cancer Sci. 112 (10) (2021) 4208–4219.
[29] H. Shen, S. Decollogne, P.J. Dilda, E. Hau, S.A. Chung, P.P. Luk, P.J. Hogg, K. L. McDonald, Dual-targeting of aberrant glucose metabolism in glioblastoma, J. Experimental Clin. Cancer Res. : CR 34 (1) (2015) 14.
[30] Y. Xia, B. Gao, X. Zhang, Targeting mitochondrial quality control of T cells: regulating the immune response in HCC, Front. Oncol. 12 (2022), 993437.
[31] M.M. Kamiński, D. Röth, P.H. Krammer, K. Gülow, Mitochondria as oxidative signaling organelles in T-cell activation: physiological role and pathological implications, Arch. Immunol. Ther. Exp. (Warsz.) 61 (5) (2013) 367–384.

[32] S.M.A. Rad, J.C. Halpin, M. Mollaei, S.W.J. Smith Bell, N. Hirankarn, A. D. McLellan, Metabolic and mitochondrial functioning in chimeric antigen receptor (car)-t cells, Cancers 13 (6) (2021).
[33] L. Guerra, L. Bonetti, D. Brenner, Metabolic modulation of immunity: a new concept in cancer immunotherapy, Cell Rep. 32 (1) (2020), 107848.
[34] A.J. Trewin, J. Silver, H.T. Dillon, P.A. Della Gatta, L. Parker, D.S. Hiam, Y.P. Lee, M. Richardson, G.D. Wadley, S. Lamon, Long non-coding RNA Tug1 modulates mitochondrial and myogenic responses to exercise in skeletal muscle, BMC Biol. 20 (1) (2022) 164.
[35] Q. Zhang, D. Li, X. Dong, X. Zhang, J. Liu, L. Peng, B. Meng, Q. Hua, X. Pei, L. Zhao, X. Hu, Y. Zhang, Z. Pan, Y. Lu, B. Yang, LncDACH1 promotes mitochondrial oxidative stress of cardiomyocytes by interacting with sirtuin3 and aggravates diabetic cardiomyopathy, Sci. China Life Sci. 65 (6) (2022) 1198–1212.
[36] Y. Yang, M. Li, Y. Liu, Z. Wang, X. Fu, X. He, Q. Wang, X.X. Li, H. Ma, K. Wang, L. Zou, J.X. Wang, T. Yu, The lncRNA punisher regulates apoptosis and mitochondrial homeostasis of vascular smooth muscle cells via targeting miR-664a-5p and OPA1, Oxid. Med. Cell. Longev. 2022 (2022) 5477024.
[37] L. Wo, X. Zhang, C. Ma, C. Zhou, J. Li, Z. Hu, X. Gong, M. Zhan, M. He, Q. Zhao, LncRNA HABON promoted liver cancer cells survival under hypoxia by inhibiting mPTP opening, Cell Death Discovery 8 (1) (2022) 171.
[38] S. Moonmuang, P. Chaiyawat, S. Jantrapirom, D. Pruksakorn, L. Lo Piccolo, Circulating long non-coding rnas as novel potential biomarkers for osteogenic sarcoma, Cancers 13 (16) (2021).
[39] L. Li, Y. Zhang, Y. Gao, Y. Hu, R. Wang, S. Wang, Y. Li, Y. He, C. Yuan, LncSNHG14 promotes nutlin3a resistance by inhibiting ferroptosis via the miR-206 /SLC7A11 axis in osteosarcoma cells, Cancer Gene Ther. (2023).
[40] Y. Wang, S. Zheng, J. Han, N. Li, R. Ji, X. Li, C. Han, W. Zhao, L. Zhang, LINC00629 protects osteosarcoma cell from ER stress-induced apoptosis and facilitates tumour progression by elevating KLF4 stability, J. Experimental Clin. Cancer Res.: CR 41 (1) (2022) 354.
[41] D. Zheng, L. Yu, Z. Wei, K. Xia, W. Guo, N6-methyladenosine-related lncrnas are potential prognostic biomarkers and correlated with tumor immune microenvironment in osteosarcoma, Front. Genet. 12 (2021), 805607.
[42] Y. Zhang, R. He, X. Lei, L. Mao, Z. Yin, X. Zhong, W. Cao, Q. Zheng, D. Li, Comprehensive analysis of a ferroptosis-related lncrna signature for predicting prognosis and immune landscape in osteosarcoma, Front. Oncol. 12 (2022), 880459.
[43] Y. He, H. Zhou, H. Xu, H. You, H. Cheng, Construction of an immune-related lncrna signature that predicts prognosis and immune microenvironment in osteosarcoma patients, Front. Oncol. 12 (2022), 769202.
[44] P. Thanindratarn, R. Wei, D.C. Dean, A. Singh, N. Federman, S.D. Nelson, F. J. Hornicek, Z. Duan, T-LAK cell-originated protein kinase (TOPK): an emerging prognostic biomarker and therapeutic target in osteosarcoma, Mol. Oncol. 15 (12) (2021) 3721–3737.
[45] Z.L. Wu, Y.J. Deng, G.Z. Zhang, E.H. Ren, W.H. Yuan, Q.Q. Xie, Development of a novel immune-related genes prognostic signature for osteosarcoma, Sci. Rep. 10 (1) (2020) 18402.
[46] H. Ma, D.C. Dean, R. Wei, F.J. Hornicek, Z. Duan, Cyclin-dependent kinase 7 (cdk7) is an emerging prognostic biomarker and therapeutic target in osteosarcoma, Therapeutic Adv. Musculoskeletal Disease 13 (2021).
[47] S. Rath, R. Sharma, R. Gupta, T. Ast, C. Chan, T.J. Durham, R.P. Goodman, Z. Grabarek, M.E. Haas, W.H.W. Hung, P.R. Joshi, A.A. Jourdain, S.H. Kim, A. V. Kotrys, S.S. Lam, J.G. McCoy, J.D. Meisel, M. Miranda, A. Panda, A. Patgiri, R. Rogers, S. Sadre, H. Shah, O.S. Skinner, T.L. To, M.A. Walker, H. Wang, P. S. Ward, J. Wengrod, C.C. Yuan, S.E. Calvo, V.K. Mootha, MitoCarta3.0: an updated mitochondrial proteome now with sub-organelle localization and pathway annotations, Nucleic Acids Res. 49 (D1) (2021) D1541–D1547.
[48] K. Liu, T. Huang, H. Zhang, H. Deng, M. Tang, Establishment and validation of a redox-related long non-coding RNAs prognostic signature in head and neck squamous cell carcinoma, Sci. Rep. 12 (1) (2022) 22040.
[49] D. Li, S. Jin, P. Chen, Y. Zhang, Y. Li, C. Zhong, X. Fan, H. Lin, Comprehensive analysis of cuproptosis-related lncRNAs for prognostic significance and immune microenvironment characterization in hepatocellular carcinoma, Front. Immunol. 13 (2022), 991604.
[50] M. Yang, H. Zheng, K. Xu, Q. Yuan, Y. Aihaiti, Y. Cai, P. Xu, A novel signature to guide osteosarcoma prognosis and immune microenvironment: cuproptosis-related lncRNA, Front. Immunol. 13 (2022), 919231.
[51] G. Chao-Yang, T. Rong, S. Yong-Qiang, L. Tai-Cong, Z. Kai-Sheng, N. Wei, Z. Hai-Hong, Prognostic signatures of metabolic genes and metabolism-related long non-coding rnas accurately predict overall survival for osteosarcoma patients, Front. Cell Dev. Biol. 9 (2021), 644220.
[52] X. Wang, C. Xie, L. Lin, Development and validation of a cuproptosis-related lncRNA model correlated to the cancer-associated fibroblasts enable the prediction prognosis of patients with osteosarcoma, J Bone Oncol 38 (2023), 100463.
[53] X. Bu, J. Liu, R. Ding, Z. Li, Prognostic value of a pyroptosis-related long noncoding rna signature associated with osteosarcoma microenvironment, J. Oncol. 2021 (2021) 2182761.
[54] P. Chen, D. Zhao, J. Li, X. Liang, J. Li, A. Chang, V.K. Henry, Z. Lan, D.J. Spring, G. Rao, Y.A. Wang, R.A. DePinho, Symbiotic macrophage-glioma cell interactions reveal synthetic lethality in pten-null glioma, Cancer Cell 35 (6) (2019) 868–884. e6.
[55] R.S. Herbst, J.C. Soria, M. Kowanetz, G.D. Fine, O. Hamid, M.S. Gordon, J. A. Sosman, D.F. McDermott, J.D. Powderly, S.N. Gettinger, H.E. Kohrt, L. Horn, D.P. Lawrence, S. Rost, M. Leabman, Y. Xiao, A. Mokatrin, H. Koeppen, P. S. Hegde, I. Mellman, D.S. Chen, F.S. Hodi, Predictive correlates of response to the anti-PD-L1 antibody MPDL3280A in cancer patients, Nature 515 (7528) (2014) 563–567.
[56] S.L. Topalian, F.S. Hodi, J.R. Brahmer, S.N. Gettinger, D.C. Smith, D. F. McDermott, J.D. Powderly, R.D. Carvajal, J.A. Sosman, M.B. Atkins, P. D. Leming, D.R. Spigel, S.J. Antonia, L. Horn, C.G. Drake, D.M. Pardoll, L. Chen, W.H. Sharfman, R.A. Anders, J.M. Taube, T.L. McMiller, H. Xu, A.J. Korman, M. Jure-Kunkel, S. Agrawal, D. McDonald, G.D. Kollia, A. Gupta, J.M. Wigginton, M. Sznol, Safety, activity, and immune correlates of anti-PD-1 antibody in cancer, N. Engl. J. Med. 366 (26) (2012) 2443–2454.
[57] R. He, H. Zhang, H. Zhao, X. Yin, J. Lu, C. Gu, J. Gao, Q. Xu, Multiomics analysis reveals cuproptosis-related signature for evaluating prognosis and immunotherapy efficacy in colorectal cancer, Cancers 15 (2) (2023).
[58] J. Jumper, R. Evans, A. Pritzel, T. Green, M. Figurnov, O. Ronneberger, K. Tunyasuvunakool, R. Bates, A. Žídek, A. Potapenko, A. Bridgland, C. Meyer, S. A.A. Kohl, A.J. Ballard, A. Cowie, B. Romera-Paredes, S. Nikolov, R. Jain, J. Adler, T. Back, S. Petersen, D. Reiman, E. Clancy, M. Zielinski, M. Steinegger, M. Pacholska, T. Berghammer, S. Bodenstein, D. Silver, O. Vinyals, A.W. Senior, K. Kavukcuoglu, P. Kohli, D. Hassabis, Highly accurate protein structure prediction with AlphaFold, Nature 596 (7873) (2021) 583–589.
[59] Y. Liu, A. Gusev, Y.J. Heng, L.B. Alexandrov, P. Kraft, Somatic mutational profiles and germline polygenic risk scores in human cancer, Genome Med. 14 (1) (2022) 14.
[60] M. Yao, P.B. Ventura, Y. Jiang, F.J. Rodriguez, L. Wang, J.S.A. Perry, Y. Yang, K. Wahl, R.B. Crittenden, M.L. Bennett, L. Qi, C.C. Gong, X.N. Li, B.A. Barres, T. P. Bender, K.S. Ravichandran, K.A. Janes, C.G. Eberhart, H. Zong, Astrocytic trans-differentiation completes a multicellular paracrine feedback loop required for medulloblastoma tumor growth, Cell 180 (3) (2020) 502–520.e19.
[61] D. Chowell, L.G.T. Morris, C.M. Grigg, J.K. Weber, R.M. Samstein, V. Makarov, F. Kuo, S.M. Kendall, D. Requena, N. Riaz, B. Greenbaum, J. Carroll, E. Garon, D. M. Hyman, A. Zehir, D. Solit, M. Berger, R. Zhou, N.A. Rizvi, T.A. Chan, Patient HLA Class I Genotype Influences Cancer Response to Checkpoint Blockade Immunotherapy, Science 359 (2018) 582–587.
[62] S. Pagliuca, C. Gurnari, M.T. Rubio, V. Visconte, T.L. Lenz, Individual HLA heterogeneity and its implications for cellular immune evasion in cancer and beyond, Front. Immunol. 13 (2022), 944872.
[63] V. Thorsson, D.L. Gibbs, S.D. Brown, D. Wolf, D.S. Bortone, T.H. Ou Yang, E. Porta-Pardo, G.F. Gao, C.L. Plaisier, J.A. Eddy, E. Ziv, A.C. Culhane, E.O. Paull, I.K.A. Sivakumar, A.J. Gentles, R. Malhotra, F. Farshidfar, A. Colaprico, J. S. Parker, L.E. Mose, N.S. Vo, J. Liu, Y. Liu, J. Rader, V. Dhankani, S.M. Reynolds, R. Bowlby, A. Califano, A.D. Cherniack, D. Anastassiou, D. Bedognetti, Y. Mokrab, A.M. Newman, A. Rao, K. Chen, A. Krasnitz, H. Hu, T.M. Malta, H. Noushmehr, C. S. Pedamallu, S. Bullman, A.I. Ojesina, A. Lamb, W. Zhou, H. Shen, T.K. Choueiri, J.N. Weinstein, J. Guinney, J. Saltz, R.A. Holt, C.S. Rabkin, A.J. Lazar, J. S. Serody, E.G 48 (Immunity 2018,) 812–830.e14. Disis, B.G. Vincent, I. Shmulevich, The Immune Landscape of Cancer.
[64] H. Ma, C. He, Y. Cheng, D. Li, Y. Gong, J. Liu, H. Tian, X. Chen, PLK1shRNA and doxorubicin co-loaded thermosensitive PLGA-PEG-PLGA hydrogels for osteosarcoma treatment, Biomaterials 35 (30) (2014) 8723–8734.
[65] Y. Zhang, W. Gan, N. Ru, Z. Xue, W. Chen, Z. Chen, H. Wang, X. Zheng, Comprehensive multi-omics analysis reveals m7G-related signature for evaluating prognosis and immunotherapy efficacy in osteosarcoma, J Bone Oncol 40 (2023), 100481.
[66] E. Urciuoli, S. Petrini, V. D'Oria, M. Leopizzi, C.D. Rocca, B. Peruzzi, Nuclear lamins and emerin are differentially expressed in osteosarcoma cells and scale with tumor aggressiveness, Cancers 12 (2) (2020).
[67] J.W.V. de Azevedo, T.A.A. de Medeiros Fernandes, J.V. Fernandes Jr., J.C.V. de Azevedo, D.C.F. Lanza, C.M. Bezerra, V.S. Andrade, J.M.G. de Araújo, J. V. Fernandes, Biology and pathogenesis of human osteosarcoma, Oncol. Lett. 19 (2) (2020) 1099–1116.
[68] G. He, J.J. Nie, X. Liu, Z. Ding, P. Luo, Y. Liu, B.W. Zhang, R. Wang, X. Liu, Y. Hai, D.F. Chen, Zinc oxide nanoparticles inhibit osteosarcoma metastasis by downregulating β-catenin via HIF-1α/BNIP3/LC3B-mediated mitophagy pathway, Bioact. Mater. 19 (2023) 690–702.
[69] T. Sun, Z. Liu, Q. Yang, The role of ubiquitination and deubiquitination in cancer metabolism, Mol. Cancer 19 (1) (2020) 146.
[70] N.M. Niemi, G.M. Wilson, K.A. Overmyer, F.N. Vögtle, L. Myketin, D.C. Lohman, K.L. Schueler, A.D. Attie, C. Meisinger, J.J. Coon, D.J. Pagliarini, Pptc7 is an essential phosphatase for promoting mammalian mitochondrial metabolism and biogenesis, Nat. Commun. 10 (1) (2019) 3197.
[71] Z. Wu, I. Tantray, J. Lim, S. Chen, Y. Li, Z. Davis, C. Sitron, J. Dong, S. Gispert, G. Auburger, O. Brandman, X. Bi, M. Snyder, B. Lu, MISTERMINATE mechanistically links mitochondrial dysfunction with proteostasis failure, Mol. Cell 75 (4) (2019) 835–848.e8.
[72] Y. Yang, S. Karakhanova, W. Hartwig, J.G. D'Haese, P.P. Philippov, J. Werner, A. V. Bazhin, Mitochondria and mitochondrial ros in cancer: novel targets for anticancer therapy, J. Cell. Physiol. 231 (12) (2016) 2570–2581.
[73] Y. Liu, C. Chen, X. Wang, Y. Sun, J. Zhang, J. Chen, Y. Shi, An epigenetic role of mitochondria in cancer, Cells 11 (16) (2022).
[74] G. Zhong, J.K. Venkatesan, H. Madry, M. Cucchiarini, Advances in human mitochondria-based therapies, Int. J. Mol. Sci. 24 (1) (2022).
[75] M.A. Dawson, T. Kouzarides, Cancer epigenetics: from mechanism to therapy, Cell 150 (1) (2012) 12–27.
[76] P. Holvoet, Noncoding RNAs controlling oxidative stress in cancer, Cancers 15 (4) (2023).

[77] K. Li, B. Zhao, D. Wei, Y. Cui, L. Qian, W. Wang, G. Liu, Long non-coding RNA ANRIL enhances mitochondrial function of hepatocellular carcinoma by regulating the MiR-199a-5p/ARL2 axis, Environ. Toxicol. 35 (3) (2020) 313–321.
[78] X. Dong, Q. Pi, A. Yuemaierabola, W. Guo, H. Tian, Silencing LINC00294 restores mitochondrial function and inhibits apoptosis of glioma cells under hypoxia via the mir-21-5p/caskin1/camp axis, Oxid. Med. Cell. Longev. 2021 (2021) 8240015.
[79] F. Galli, J.V. Aguilera, B. Palermo, S.N. Markovic, P. Nisticò, A. Signore, Relevance of immune cell and tumor microenvironment imaging in the new era of immunotherapy, J. Experimental Clin. Cancer Res.: CR 39 (1) (2020) 89.
[80] D.S. Chen, I. Mellman, Elements of cancer immunity and the cancer-immune set point, Nature 541 (7637) (2017) 321–330.
[81] C.L. Kuo, A. Ponneri Babuharisankar, Y.C. Lin, H.W. Lien, Y.K. Lo, H.Y. Chou, V. Tangeda, L.C. Cheng, A.N. Cheng, A.Y. Lee, Mitochondrial oxidative stress in the tumor microenvironment and cancer immunoescape: foe or friend? J. Biomed. Sci. 29 (1) (2022) 74.
[82] N.E. Scharping, A.V. Menk, R.S. Moreci, R.D. Whetstone, R.E. Dadey, S. C. Watkins, R.L. Ferris, G.M. Delgoffe, The tumor microenvironment represses t cell mitochondrial biogenesis to drive intratumoral t cell metabolic insufficiency and dysfunction, Immunity 45 (3) (2016) 701–703.
[83] C.S. Field, F. Baixauli, R.L. Kyle, D.J. Puleston, A.M. Cameron, D.E. Sanin, K. L. Hippen, M. Loschi, G. Thangavelu, M. Corrado, J. Edwards-Hicks, K.M. Grzes, E.J. Pearce, B.R. Blazar, E.L. Pearce, Mitochondrial integrity regulated by lipid metabolism is a cell-intrinsic checkpoint for treg suppressive function, Cell Metab. 31 (2) (2020) 422–437.e5.
[84] N.P. Restifo, M.E. Dudley, S.A. Rosenberg, Adoptive immunotherapy for cancer: harnessing the T cell response, Nat. Rev. Immunol. 12 (4) (2012) 269–281.
[85] S.A. Rosenberg, N.P. Restifo, Adoptive Cell Transfer as Personalized Immunotherapy for Human Cancer, Science 348 (2015) 62–68.
[86] C. Wang, M. Li, R. Wei, J. Wu, Adoptive transfer of TILs plus anti-PD1 therapy: an alternative combination therapy for treating metastatic osteosarcoma, J Bone Oncol 25 (2020), 100332.
[87] N. Rainusso, V.S. Brawley, A. Ghazi, M.J. Hicks, S. Gottschalk, J.M. Rosen, N. Ahmed, Immunotherapy targeting HER2 with genetically modified T cells eliminates tumor-initiating cells in osteosarcoma, Cancer Gene Ther. 19 (3) (2012) 212–217.
[88] F.F. Hu, C.J. Liu, L.L. Liu, Q. Zhang, A.Y. Guo, Expression profile of immune checkpoint genes and their roles in predicting immunotherapy response, Brief. Bioinform. 22 (3) (2021).
[89] S. Mukherjee, G.K. Bhatti, R. Chhabra, P.H. Reddy, J.S. Bhatti, Targeting mitochondria as a potential therapeutic strategy against chemoresistance in cancer, Biomedicine & Pharmacotherapy = Biomedecine & Pharmacotherapie 160 (2023), 114398.
[90] F. Guerra, A.A. Arbini, L. Moro, Mitochondria and cancer chemoresistance, Biochimica et biophysica acta, Bioenergetics 1858 (8) (2017) 686–699.
[91] Y. Li, Y. Gan, J. Liu, J. Li, Z. Zhou, R. Tian, R. Sun, J. Liu, Q. Xiao, Y. Li, P. Lu, Y. Peng, Y. Peng, G. Shu, G. Yin, Downregulation of MEIS1 mediated by ELFN1-AS1/EZH2/DNMT3a axis promotes tumorigenesis and oxaliplatin resistance in colorectal cancer, Signal Transduct. Target. Ther. 7 (1) (2022) 87.
[92] W. Feng, R. Zhu, J. Ma, H. Song, LncRNA ELFN1-AS1 Promotes Retinoblastoma Growth and Invasion via Regulating miR-4270/SBK1 Axis, Cancer Manag. Res. 13 (2021) 1067–1073.
[93] G. Ma, G. Li, A. Gou, Z. Xiao, Y. Xu, S. Song, K. Guo, Z. Liu, Long non-coding RNA ELFN1-AS1 in the pathogenesis of pancreatic cancer, Annals Trans. Med. 9 (10) (2021) 877.
[94] Y. Jie, L. Ye, H. Chen, X. Yu, L. Cai, W. He, Y. Fu, ELFN1-AS1 accelerates cell proliferation, invasion and migration via regulating miR-497-3p/CLDN4 axis in ovarian cancer, Bioengineered 11 (1) (2020) 872–882.
[95] B. Yang, S. Miao, lncRNA ELFN1-AS1 predicts poor prognosis and promotes tumor progression of non-small cell lung cancer by sponging miR-497, Cancer Biomarkers : Section A of Disease Markers 34 (4) (2022) 637–646.
[96] B. Wang, X. Wang, P. Li, X. Niu, X. Liang, G. Liu, Z. Liu, H. Ge, Osteosarcoma cell-derived exosomal elfn1-as1 mediates macrophage m2 polarization via sponging mir-138-5p and mir-1291 to promote the tumorgenesis of osteosarcoma, Front. Oncol. 12 (2022), 881022.
[97] G. Wang, X. Zhang, W. Feng, J. Wang, Prediction of prognosis and immunotherapy of osteosarcoma based on necroptosis-related lncRNAs, Front. Genet. 13 (2022), 917935.
[98] W. Jiang, Y. He, W. He, G. Wu, X. Zhou, Q. Sheng, W. Zhong, Y. Lu, Y. Ding, Q. Lu, F. Ye, H. Hua, Exhausted CD8+T cells in the tumor immune microenvironment: new pathways to therapy, Front. Immunol. 11 (2020), 622509.
[99] Y.R. Yu, H. Imrichova, H. Wang, T. Chao, Z. Xiao, M. Gao, M. Rincon-Restrepo, F. Franco, R. Genolet, W.C. Cheng, C. Jandus, G. Coukos, Y.F. Jiang, J. W. Locasale, A. Zippelius, P.S. Liu, L. Tang, C. Bock, N. Vannini, P.C. Ho, Disturbed mitochondrial dynamics in CD8(+) TILs reinforce T cell exhaustion, Nat. Immunol. 21 (12) (2020) 1540–1551.
[100] M. Reina-Campos, N.E. Scharping, A.W. Goldrath, CD8(+) T cell metabolism in infection and cancer, Nat. Rev. Immunol. 21 (11) (2021) 718–738.
[101] G.V. Sharonov, E.O. Serebrovskaya, D.V. Yuzhakova, O.V. Britanova, D. M. Chudakov, B cells, plasma cells and antibody repertoires in the tumour microenvironment, Nat. Rev. Immunol. 20 (5) (2020) 294–307.
[102] F. Hong, Z. Gong, X. Zhang, P. Ma, Y. Yin, H. Wang, Identification of biomarkers and ceRNA network in glioblastoma through bioinformatic analysis and evaluation of potential prognostic values, Annals Trans. Med. 9 (20) (2021) 1561.
[103] Y. Jiang, X. Gou, Z. Wei, J. Tan, H. Yu, X. Zhou, X. Li, Bioinformatics profiling integrating a three immune-related long non-coding RNA signature as a prognostic model for clear cell renal cell carcinoma, Cancer Cell Int. 20 (2020) 166.
[104] Y. Wang, Y. Zhao, W. Guo, G.S. Yadav, C. Bhaskarla, Z. Wang, X. Wang, S. Li, Y. Wang, Y. Chen, D. Pattarayan, W. Xie, S. Li, B. Lu, U.S. Kammula, M. Zhang, D. Yang, Genome-wide gain-of-function screening characterized lncRNA regulators for tumor immune response, Sci. Adv. 8 (49) (2022) eadd0005.
[105] J. Zhang, R. Ding, T. Wu, J. Jia, X. Cheng, Autophagy-related genes and long noncoding rnas signatures as predictive biomarkers for osteosarcoma survival, Front. Cell Dev. Biol. 9 (2021), 705291.
[106] H. Gao, Y. Guo, M. Zhang, Z. Yi, Comprehensive characterization of prognostic long noncoding rnas in osteosarcoma, Biomed Res. Int. 2020 (2020) 6725753.
[107] J. Liu, Q. Liu, H. Shen, Y. Liu, Y. Wang, G. Wang, J. Du, Identification and validation of a three pyroptosis-related lncrna signature for prognosis prediction in lung adenocarcinoma, Front. Genet. 13 (2022), 838624.
[108] Y. Guo, Z. Qu, D. Li, F. Bai, J. Xing, Q. Ding, J. Zhou, L. Yao, Q. Xu, Identification of a prognostic ferroptosis-related lncRNA signature in the tumor microenvironment of lung adenocarcinoma, Cell Death Discovery 7 (1) (2021) 190.
[109] L. Wu, Z. Wen, Y. Song, L. Wang, A novel autophagy-related lncRNA survival model for lung adenocarcinoma, J. Cell Mol. Med. 25 (12) (2021) 5681–5690.
[110] T.M. Malta, A. Sokolov, A.J. Gentles, T. Burzykowski, L. Poisson, J.N. Weinstein, B. Kamińska, J. Huelsken, L. Omberg, O. Gevaert, A. Colaprico, P. Czerwińska, S. Mazurek, L. Mishra, H. Heyn, A. Krasnitz, A.K. Godwin, A.J. Lazar, J.M. Stuart, K.A. Hoadley, P.W. Laird, H. Noushmehr, M. Wiznerowicz, Machine learning identifies stemness features associated with oncogenic dedifferentiation, Cell 173 (2) (2018) 338–354.e15.
[111] J. Pu, W. Li, A. Wang, Y. Zhang, Z. Qin, Z. Xu, J. Wang, Y. Lu, Q. Tang, H. Wei, Long non-coding RNA HOMER3-AS1 drives hepatocellular carcinoma progression via modulating the behaviors of both tumor cells and macrophages, Cell Death Dis. 12 (12) (2021) 1103.
[112] K.F. Chan, J.D.G. Duarte, S. Ostrouska, A. Behren, γδ T cells in the tumor microenvironment-interactions with other immune cells, Front. Immunol. 13 (2022), 894315.
[113] B. Silva-Santos, K. Serre, H. Norell, γδ T cells in cancer, Nat. Rev. Immunol. 15 (11) (2015) 683–691.
[114] K. Yan, T.T. Da, Z.H. Bian, Y. He, M.C. Liu, Q.Z. Liu, J. Long, L. Li, C.Y. Gao, S. H. Yang, Z.B. Zhao, Z.X. Lian, Multi-omics analysis identifies FoxO1 as a regulator of macrophage function through metabolic reprogramming, Cell Death Dis. 11 (9) (2020) 800.
[115] K.M. Bussard, L. Mutkus, K. Stumpf, C. Gomez-Manzano, F.C. Marini, Tumor-associated stromal cells as key contributors to the tumor microenvironment, Breast Cancer Research : BCR 18 (1) (2016) 84.
[116] C. Kerneur, C.E. Cano, D. Olive, Major pathways involved in macrophage polarization in cancer, Front. Immunol. 13 (2022) 1026954.